



1 Changes of air pollutant emissions in China during two clean air 2 action periods derived from the newly developed Inversed Emission 3 Inventory for Chinese Air Quality (CAQIEI)

4 Lei Kong^{1,3}, Xiao Tang^{*,1,3}, Zifa Wang^{*,1,3,4}, Jiang Zhu^{1,2}, Jianjun Li⁵, Huangjian Wu^{1,3}, Qizhong Wu⁶,
5 Huansheng Chen^{1,3}, Lili Zhu⁵, Wei Wang⁵, Bing Liu⁵, Qian Wang⁷, Duohong Chen⁸, Yuepeng Pan^{1,3}, Jie
6 Li^{1,3}, Lin Wu^{1,3}, and Gregory R. Carmichael⁹

7 ¹State Key Laboratory of Atmospheric Boundary Layer Physics and Atmospheric Chemistry (LAPC), Institute of Atmospheric
8 Physics, Chinese Academy of Sciences, Beijing 100029, China

9 ²CAS-TWAS Center of Excellence for Climate and Environment Sciences (ICCES), Institute of Atmospheric Physics, Chinese
10 Academy of Sciences, Beijing 100029, China

11 ³College of Earth and Planetary Sciences, University of Chinese Academy of Sciences, Beijing 100049, China

12 ⁴Center for Excellence in Regional Atmospheric Environment, Institute of Urban Environment, Chinese Academy of Sciences,
13 Xiamen 361021, China

14 ⁵China National Environmental Monitoring Centre, Beijing, 100012, China

15 ⁶College of Global Change and Earth System Science, Faculty of Geographical Science, Beijing Normal University, Beijing
16 100875, China

17 ⁷Shanghai Environmental Monitoring Centre, Shanghai, 200030, China

18 ⁸Guangdong Ecological Environment Monitoring Centre, National Key Laboratory of Regional Air Quality Monitoring for
19 Environmental Protection, Guangzhou 510308, China

20 ⁹Center for Global and Regional Environmental Research, University of Iowa, Iowa City, IA 52242, USA

21 *Correspondence to:* Xiao Tang (tangxiao@mail.iap.ac.cn) and Zifa Wang (zifawang@mail.iap.ac.cn)

22 Abstract

23 A new long-term emission inventory called the Inversed Emission Inventory for Chinese Air Quality (CAQIEI) was developed
24 in this study by assimilating surface observations from the China National Environmental Monitoring Centre (CNEMC) using
25 the ensemble Kalman filter (EnKF) and the Nested Air Quality Prediction Modeling System (NAQPMS). This inventory
26 contains the constrained monthly emissions of NO_x, SO₂, CO, primary PM_{2.5}, primary PM₁₀, and NMVOCs in China from
27 2013 to 2020, with a horizontal resolution of 15 km × 15 km. This paper documents detailed descriptions of the assimilation
28 system and the evaluation results for the emission inventory. The results suggest that CAQIEI can effectively reduce the biases
29 in the *a priori* emission inventory, with the normalized mean biases ranging from −9.1% to 9.5% in the *a posteriori* simulation,
30 which are significantly reduced from the biases in the *a priori* simulations (−45.6% to 93.8%). The calculated RMSEs (0.3
31 mg/m³ for CO and 9.4–21.1 µg/m³ for other species, on the monthly scale) and correlation coefficients (0.76–0.94) were also
32 improved from the *a priori* simulations, suggesting that CAQIEI can reasonably reproduce the magnitude and variation of
33 emissions of different air pollutants in China. Based on CAQIEI, we estimated China's total emissions (including both natural
34 and anthropogenic emissions) of the 6 species in 2015 to be as follows: 25.2 Tg of NO_x, 17.8 Tg of SO₂, 465.4 Tg of CO, 15.0
35 Tg of PM_{2.5}, 40.1 Tg of PM₁₀, and 46.0 Tg of NMVOCs. From 2015 to 2020, the total emissions reduced by 54.1% for SO₂,
36 44.4% for PM_{2.5}, 33.6% for PM₁₀, 35.7% for CO, and 15.1% for NO_x, but increased by 21.0% for NMVOCs. Larger emission
37 reductions were achieved during the 2018–2020 action plan than during the 2013–2017 action plan for most species. In
38 particular, NO_x and NMVOC emissions were shown to increase during the 2013–2017 action plan, and there were obvious
39 emission increases in the Fengwei Plain area over the Central China region. However, NO_x and NMVOC emissions declined
40 during the 2018–2020 action plan, and the emissions over the Fengwei Plain area also decreased. This suggests that the
41 emission control policies were improved in the 2018–2020 action plan. We also compared CAQIEI with previous inventories,
42 which verified our inversion results in terms of total emissions of NO_x, SO₂ and NMVOCs, and more importantly identified
43 the potential uncertainties in our current understanding of China's air pollutant emissions. Firstly, CO emissions in China may
44 be substantially underestimated by current inventories, with the CO emissions estimated by CAQIEI (426.8 Tg) being more



45 than twice the amount in previous inventories (120.7–237.7 Tg). Significant underestimations for other air pollutant emissions
46 may also exist over western and northeastern China. In addition, the NMVOC emissions were shown to be substantially
47 underestimated over northern China but overestimated in southern China. Secondly, the emission reduction rates during 2015–
48 2018 estimated by CAQIEI are generally smaller than those estimated by previous inventories, especially for NO_x, PM₁₀ and
49 NMVOCs, suggesting that the mitigation effects of the air pollution control may be overestimated currently. In particular,
50 China’s NMVOC emissions were shown to have increased by 26.6% from 2015 to 2018, especially over the North China Plain
51 (by 38.0%), Northeast China (by 38.3%), and Central China (60.0%). In contrast, the emissions reduction rate of CO may be
52 underestimated. Overall, our emissions inventory sheds new light on the complex variations of air pollutant emissions in China
53 during its two recent clean air action periods, which could significantly improve our understanding of air pollutant emissions
54 and related changes in air quality in China. The datasets are available at <https://doi.org/10.57760/sciencedb.13151> (Kong et
55 al., 2023).

56 1 Introduction

57 Air pollution is a serious environmental issue owing to its substantial impacts on human health, ecosystems, and climate
58 change (Von Schneidmesser et al., 2015; Cohen et al., 2017; Bobbink et al., 1998). According to the World Health
59 Organization, air pollution–induced strokes, lung cancer, and heart disease are causing millions of premature deaths worldwide
60 every year (WHO, 2016). The fine particulate matter (PM_{2.5}) in the atmosphere not only degrades visibility but also affects the
61 radiative forcing of the climate, both directly and indirectly (Martin et al., 2004). After removal from the atmosphere through
62 dry and wet deposition, air pollutants such as sulfur, nitrate, and ammonium contribute significantly to soil acidification,
63 eutrophication, and even biodiversity reduction (Krupa, 2003; Hernández et al., 2016).

64 China has experienced severe PM_{2.5} pollution in recent decades, due to its large emissions of air pollutants associated
65 with rapid urbanization and high consumption of fossil fuels (Kan et al., 2012; Song et al., 2017). The annual concentrations
66 of PM_{2.5} in 2013 reached 106, 67 and 47 µg/m³ over the Beijing–Tianjin–Hebei, Yangtze River Delta, and Peral River Delta
67 region, respectively, which were all higher than China’s national standard (35 µg/m³), and 5–10 times higher than that of the
68 World Health Organization (10 µg/m³). To tackle this problem, strict emission control policies (so-called “clean air action
69 plans”) have been proposed by China’s government, including the “Action Plan on the Prevention and Control of Air Pollution”
70 from 2013 to 2017 (hereinafter called the “2013–2017 Action Plan”), and the “Three-year Action Plan for Winning the Blue
71 Sky War” from 2018–2020 (hereinafter called the “2018–2020 Action Plan”). With the successful implementation of these
72 two action plans, the air quality was substantially improved in China, as evidenced in both observational and reanalysis datasets
73 (Li et al., 2020b; Zheng et al., 2017; Krotkov et al., 2016; Zhong et al., 2021; Li et al., 2017a; Kong et al., 2021). However,
74 with the deepening of air pollution control, unexpected changes have occurred in China, bringing about new challenges for the
75 mitigation of air pollution in the future. On the one hand, despite a significant decline in PM_{2.5} concentrations in China, severe
76 haze still occasionally occurs during the wintertime (Zhou et al., 2022b; Li et al., 2017c). In addition, field measurements in
77 cities over different regions of China consistently show different responses of aerosol chemical compositions to the emission
78 control policies (Tang et al., 2021; Zhou et al., 2019; Wang et al., 2022; Zhang et al., 2020; Li et al., 2019a; Xu et al., 2019b;
79 Lei et al., 2021; Zhou et al., 2022a). Compared with other aerosol species that show substantial decreases during the clean air
80 action plans, nitrate has shown a weaker response to the control measures, remaining at high levels and in some cases having
81 even increased slightly. As a result, nitrate is playing an increasingly important role in heavy haze episodes in winter, and
82 dominates the chemical composition of PM_{2.5} (Fu et al., 2020; Xu et al., 2019a), leading to a rapid transition from sulphate- to
83 nitrate-driven aerosol pollution (Li et al., 2019a; Wang et al., 2019b). On the other hand, photochemical pollution has
84 deteriorated in China, with ozone (O₃) concentrations having increased substantially in eastern China during 2013–2017 (Li et
85 al., 2019b; Lu et al., 2018; Lu et al., 2020; Wang et al., 2020b).



86 These unexpected changes have raised considerable concern among the scientific community and policymakers regarding
87 the overall effects of the clean air action plans, and how to coordinate the control of PM_{2.5} and O₃ pollution. Addressing this
88 problem requires a comprehensive understanding of the effects of the clean air action plans on the emissions of different
89 chemical species. In this respect, previous studies have compiled several long-term air pollutant emission inventories in China
90 using the bottom-up approach – for example, the Multi-resolution Emission Inventory for China (MEIC) developed by
91 Tsinghua University for 2010–2020 (Zheng et al., 2018); the Air Benefit and Cost and Attainment Assessment System-
92 Emission Inventory version 2.0 (ABaCAS-EI v2.0) developed by Tsinghua University for 2005–2021 (Li et al., 2023); the
93 Regional Emission Inventory in Asia (REAS) for 1950–2015 developed Kurokawa and Ohara (2020); the Emissions Database
94 for Global Atmospheric Research (EDGAR) for 1970–2018 developed by Jalkanen et al. (2012); the Hemispheric Transport
95 of Air Pollution (HTAP) Inventory for 2000–2018 developed by Crippa et al. (2023); and the Community Emissions Data
96 System (CEDS) Inventory for 1970–2019 developed by McDuffie et al. (2020). These emission inventories have provided the
97 community with important insights into the long-term changes in the emissions of different air pollutants in China, thus playing
98 an indispensable role in our understanding of the effects of the country’s clean air action plans on emissions and air quality.
99 However, due to the lack of accurate activity data and emission factors, bottom-up emission inventories are still subject to
100 large uncertainties, particularly during the clean air action periods when the activity data and emission factors changed
101 considerably and were difficult to track. Consequently, the estimated emission rates from different bottom-up emission
102 inventories could differ by more than a factor of 2 (Elguindi et al., 2020). For example, the estimated emissions for the year
103 2010 from different bottom-up inventories were 104.9–194.5 Tg for carbon monoxide (CO), 15.6–25.4 Tg for nitrogen oxides
104 (NO_x), 22.9–27.0 Tg for non-methane volatile organic compounds (NMVOCs), 15.7–35.5 Tg for sulfur dioxide (SO₂), 1.28–
105 2.34 Tg for black carbon (BC), and 2.78–4.66 Tg for organic carbon (OC), reflecting the large uncertainty in current bottom-
106 up estimates of air pollutant emissions in China, which hinders the proper assessment of the effects of the clean air action
107 plans.

108 Inverse modeling of multiple air pollutant emissions (i.e., a top-down approach) provides an attractive way to constrain
109 bottom-up emissions by reducing the discrepancy between the model and observation through the use of data assimilation.
110 Numerous studies have confirmed the effectiveness of such a top-down method in verifying bottom-up emission estimates and
111 reducing their uncertainties (e.g., Elbern et al., 2007; Henze et al., 2009; Miyazaki and Eskes, 2013; Tang et al., 2013; Koohkan
112 et al., 2013; Koukoulis et al., 2018; Jiang et al., 2017; Muller et al., 2018; Paulot et al., 2014; Qu et al., 2017. Based on long-
113 term satellite observations, the top-down method has also been used to track the long-term variations of emissions. For example,
114 Zheng et al. (2019) estimated the global emissions of CO for the period 2000–2017 based on a multi-species atmospheric
115 Bayesian inversion approach; Qu et al. (2019) constrained global SO₂ emissions for the period 2005–2017 by assimilating
116 satellite retrievals of SO₂ columns using a hybrid 4DVar/mass balance emission inversion method; by assimilating satellite
117 observations of multiple species, Miyazaki et al. (2020b) simultaneously estimated global emissions of CO, NO_x, and SO₂ for
118 the period 2005–2018; and, most recently, a regional top-down estimation of PM_{2.5} emissions in China during 2016–2020 was
119 carried out by Peng et al. (2023) by assimilating surface observations. These studies provide us with valuable clues for
120 evaluating bottom-up emissions and improving our knowledge on the changes in emissions of different species in China during
121 the clean air action plans. However, most of these studies focused on emission trends at the global scale, which involved the
122 use of coarse model resolutions (>1°) that may be insufficient to capture the spatial variability of emission variations at the
123 regional scale. Meanwhile, current long-term, top-down estimates mainly focus on single species and do not fully cover the
124 two clean air action periods in China. Indeed, to date, there are still no long-term, top-down estimates of major air pollutant
125 emissions in China that fully cover the two clean air action periods.

126 In a previous study performed by our group, we developed a high-resolution air quality reanalysis dataset over China
127 (CAQRA) for the period 2013–2020 to track the air quality trends in China during the clean air action periods (Kong et al.,
128 2021). In the present study, as a follow up to this work, we constrained the long-term emission trends of major air pollutants



129 in China for 2013–2020 (which will be extended in the future on a yearly basis) by assimilating surface observations of air
130 pollutants from the China National Environmental Monitoring Centre (CNEMC) using an ensemble Kalman filter and the
131 Nested Air Quality Prediction and Forecasting System (NAQPMS). In the following sections, we present detailed descriptions
132 of the chemical data assimilation, the evaluation results of the inversed emissions inventory, and the estimated emission trends
133 of different air pollutants in China during the clean air action periods.

134 **2 The chemical data assimilation system**

135 We used the chemical data assimilation system (ChemDAS) developed by the Institute of Atmospheric Physics, Chinese
136 Academy of Sciences, to constrain the long-term emission trends of different air pollutants in China, which was used in the
137 development of CAQRA in our previous work (Kong et al., 2021). Since the chemical transport model (CTM) and the
138 observations used in the top-down estimation were the same as those used in CAQRA, we only briefly describe these two
139 components in the following two subsections, instead concentrating on providing a fuller description (in the third subsection)
140 of the inversion scheme in ChemDAS.

141 **2.1 Chemical transport model**

142 The NAQPMS model was used as the forecast model to represent the atmospheric chemistry in this study, and the Weather
143 Research and Forecasting (WRF) model was used as the meteorological model to provide the meteorological input data.
144 NAQPMS contains comprehensive modules for the emission, diffusion, transportation, deposition, and chemistry processes in
145 the atmosphere, and has been used in previous inversion studies (Tang et al., 2013; Kong et al., 2019; Wu et al., 2020a; Kong
146 et al., 2023). Detailed configurations of the different modules used in NAQPMS are available in these publications.

147 Figure 1 shows the domain of the inverse model, which is the same as that used in CAQRA, with a fine-scale horizontal
148 resolution of 15 km. The *a priori* emissions inventory includes the anthropogenic emissions obtained from the HTAP v2.2
149 emissions inventory, with a base year of 2010 (Janssens-Maenhout et al., 2015); biogenic emissions obtained from the
150 Monitoring Atmospheric Composition and Climate (MACC) project (Sindelarova et al., 2014); biomass burning emissions
151 obtained from the Global Fire Emissions Database (GFED), version 4 (Van Der Werf et al., 2010; Randerson et al., 2017); soil
152 and lightning NO_x emissions obtained from Yan et al. (2003) and Price et al. (1997); and marine volatile organic compound
153 emissions obtained from the POET database (Granier et al., 2005). The dust emissions were calculated online in NAQPMS as
154 a function of the relative humidity, frictional velocity, mineral particle size distribution, and the surface roughness (Li et al.,
155 2012), while the sea salt emissions were calculated using the scheme of Athanasopoulou et al. (2008). Note that we did not
156 consider the temporal variation in the *a priori* emission inventory, so that the top-down estimated emission trends were only
157 derived from the surface observations. The initial condition was treated as clean air in NAQPMS, with a 2-week spin-up time.
158 Top and boundary conditions were provided by the Model for Ozone and Related Chemical Tracers (MOZART) (Brasseur et
159 al., 1998; Hauglustaine et al., 1998). To improve the performance of meteorological simulation, a 36-h free run of the WRF
160 model was conducted for each day by using the NCAR/NCEP 1°×1° reanalysis data. The simulation results of the first 12 h
161 were treated as the spin-up run, and the remaining 24 h were used to provide the meteorological inputs for the NAQPMS
162 model.

163 **2.2 Assimilated observations**

164 The assimilated observational dataset in this study was the same as that used in CAQRA, which includes surface
165 concentrations of PM_{2.5}, PM₁₀ (coarse particulate matter), SO₂, NO₂ (nitrogen dioxide), CO, and O₃, from 2013 to 2020,
166 obtained from CNEMC (Fig. 1). Before the assimilation, outliers of the observations were filtered out by using an automatic
167 quality control method developed by Wu et al. (2018). Four types of outliers characterized by temporal and spatial



168 inconsistencies, instrument-induced low variances, periodic calibration exceptions, and lower PM₁₀ concentrations than those
169 of PM_{2.5}, were filtered out to prevent adverse impacts on the inversion process. As estimated in Kong et al. (2021), about 1.5%
170 of observational data were filtered out after quality control, but further assessment showed that it had few effects on the average
171 concentrations of different species, which were estimated to be less than 1 µg/m³ for the gaseous air pollutants and less than
172 5 µg/m³ for the particulate matter. Estimation of observation error is also important to the inversion of emissions since the
173 observational error and background errors determine the degree of adjustment to the emissions. The observational error
174 comprises the measurement error and the representativeness error induced by the different spatial scales that the model and
175 observations represent. The estimations of these two components of observational error were the same as those used in CAQRA,
176 detailed descriptions of which are available in Kong et al. (2021).

177 It should be noted that the number of observation sites were not constant throughout the whole inversion period, being
178 approximately 510 in 2013 and then increasing to 1436 in 2015, which could lead to spurious trends in the top-down estimated
179 emissions. To investigate the potential impacts of this on the top-down estimations, the changes in the coverage of observations
180 over different regions of China from 2013 to 2020 were calculated by the ratio of areas that were influenced by observations
181 to the total area of each region (Fig. 2). It can be clearly seen that the observational coverage increased from 2013 to 2015 with
182 the expansion of the air quality monitoring network in China, and became stable after 2015. However, the influence of the
183 variation in the number of observation sites varied among different regions. Over the North China Plain (NCP) region, the
184 observational coverage was approximately 90% in 2013, and reached 100% in 2014, suggesting that the variation in the
185 observation sites may have little influence on the estimated changes in emissions there. A similar conclusion can be drawn for
186 the Southeast China (SE) region, where the observational coverage was about 75% in 2013 and reached 100% in 2015.
187 Elsewhere, in the other four regions, the influence of the variation in observation sites is expected to be larger because of the
188 low observational coverage in both 2013 and 2014. For example, the observational coverage over the Northwest China (NW)
189 region was less than 10% in 2013, but increased to about 60% in 2015. Such large changes in observational coverage are
190 believed to significantly influence the estimated changes in emissions over these regions. Thus, in order to reduce this influence
191 on the estimated emission trends, in our analysis we mainly present the emission trends after 2015, when the observational
192 coverage had stabilized in all regions.

193 2.3 Data assimilation algorithm

194 We used the modified EnKF coupled with state augmentation method to constrain the long-term emissions of different
195 air pollutants. EnKF is an advanced data assimilation method originally proposed by Evensen (1994) that features representing
196 the background error covariance matrix with a stochastic ensemble of model realizations. Through the use of ensemble
197 simulations, it has the ability to consider the indirect relationship between the emissions and chemical concentrations caused
198 by the complex physical and chemical processes in the atmosphere. It also allows for the estimation of flow-dependent
199 emission–concentration relationships that vary in time and space depending on the atmospheric conditions. The modified
200 EnKF is an offline application of the EnKF method that works by decoupling the analysis step from the ensemble simulation,
201 which has benefits in the reuse of costly ensemble simulations and makes high-resolution long-term inversion affordable (Wu
202 et al., 2020a). The state augmentation method is a commonly used parameter estimation method (Tandeo et al., 2020) in which
203 the air pollutant emissions are taken as the state variable and are updated according to the error covariance between the
204 emissions and the concentrations of related species.

205 2.3.1 State variable and ensemble generations

206 The state variable used in this study was chosen following our previous multi-species inversion study (Kong et al., 2023),
207 which included the scaling factors for the emissions of fine-mode unspicuated aerosol (PMF), coarse-mode unspicuated aerosol



208 (PMC), BC, OC, NO_x, SO₂, CO, and NMVOCs, as well as the chemical concentrations of PM_{2.5}, PM_{10-2.5} (PM₁₀ minus PM_{2.5}),
209 NO₂, SO₂, CO, and daily maximum 8-h O₃ (MDA8h O₃), which are formulated as follows:

$$210 \mathbf{x} = [\mathbf{c}, \boldsymbol{\beta}]^T, \quad (1)$$

$$211 \mathbf{c} = [\mathbf{PM}_{2.5}, \mathbf{PM}_{10-2.5}, \mathbf{NO}_2, \mathbf{SO}_2, \mathbf{CO}, \mathbf{MDA8h O}_3], \quad (2)$$

$$212 \boldsymbol{\beta} = [\boldsymbol{\beta}_{\text{PMF}}, \boldsymbol{\beta}_{\text{PMC}}, \boldsymbol{\beta}_{\text{BC}}, \boldsymbol{\beta}_{\text{OC}}, \boldsymbol{\beta}_{\text{NO}_x}, \boldsymbol{\beta}_{\text{SO}_2}, \boldsymbol{\beta}_{\text{CO}}], \quad (3)$$

213 where \mathbf{x} denotes the vector of the state variable, \mathbf{c} denotes the vector of the chemical concentrations of different species, and
214 $\boldsymbol{\beta}$ denotes the vector of the scaling factors for the emissions of different species. Detailed descriptions of the state variables
215 are available in Table 1.

216 The ensemble of the scaling factors was generated using the same method of Kong et al. (2021), which has a medium size
217 of 50 and considers the uncertainties of major air pollutant emissions in China, including SO₂, NO_x, CO, NMVOCs, ammonia,
218 PM₁₀, PM_{2.5}, BC, and OC. The uncertainties of these species were considered to be 12%, 31%, 70%, 68%, 53%, 132%, 130%,
219 208% and 258%, respectively according to the estimates of Li et al. (2017b) and Streets et al. (2003). The ensemble of the
220 chemical concentrations was generated through an ensemble simulation based on NAQPMS and the perturbed emissions
221 calculated by multiplying the *a priori* emissions by the ensemble of the scaling factors. This treatment implicitly assumes that
222 the uncertainty in the chemical concentration is mainly caused by the emission uncertainty. This makes sense on a monthly or
223 yearly basis, considering that substantial changes in emissions are expected to have taken place during the clean air action
224 plans, which are subject to large uncertainty. However, the lack of consideration of other error sources, such as those of the
225 meteorological simulation and the model itself, may lead to underestimation of the background error covariance and
226 overcorrection of the emissions, which is a potential limitation of this study. In addition, the dust and sea salt emissions were
227 not perturbed and constrained in this study, and thus the errors in the simulated fine and coarse dust emissions would influence
228 the inversion of PM_{2.5} and PM₁₀ emissions. As a result, the top-down estimated PM_{2.5} and PM₁₀ emissions will contain errors
229 in the simulated dust and sea salt emissions. Particularly, we did not consider the emission of coarse dust during the inversion
230 process since we found large errors in the simulated coarse dust concentration that could have significantly influenced the
231 inversion of PM₁₀ emissions. Consequently, the top-down estimated PM₁₀ emissions in this study comprise all coarse dust
232 emissions. A detailed description of the ensemble generation is available in Kong et al. (2021).

233 2.3.2 Inversion algorithm

234 We used a deterministic form of EnKF (DEnKF) proposed by Sakov and Oke (2008) to update the scaling factors of the
235 emissions of different species, which is formulated as follows:

$$236 \bar{\mathbf{x}}^a = \bar{\mathbf{x}}^b + \lambda \mathbf{B}_e^b \mathbf{H}^T (\mathbf{H} \lambda \mathbf{B}_e^b \mathbf{H}^T + \mathbf{R})^{-1} (\mathbf{y}^o - \mathbf{H} \bar{\mathbf{x}}^b), \quad (2)$$

$$237 \bar{\mathbf{x}}^b = \frac{1}{N} \sum_{i=1}^N \mathbf{x}_i^b; \mathbf{X}_i^b = \mathbf{x}_i^b - \bar{\mathbf{x}}^b, \quad (3)$$

$$238 \mathbf{B}_e^b = \frac{1}{N-1} \sum_{i=1}^N \mathbf{X}_i^b (\mathbf{X}_i^b)^T, \quad (4)$$

239 where $\bar{\mathbf{x}}$ denotes the ensemble mean of the state variable; the superscript \mathbf{b} and \mathbf{a} respectively denote the *a priori* and *a*
240 *posteriori* estimate; \mathbf{B}_e^b is the background error covariance matrix calculated by the background perturbation \mathbf{X}^b ; \mathbf{y}^o is the
241 vector of the observation and \mathbf{R} is the observation error covariance matrix; \mathbf{H} is the linear observation operator, which maps
242 the model space to the observation space; λ is the inflation factor used to compensate for the underestimation of the background
243 error caused by the limited ensemble size and unaccounted error sources, which is calculated using the method of Wang and
244 Bishop (2003),

$$245 \lambda = \frac{(\mathbf{R}^{-1/2} \mathbf{d})^T \mathbf{R}^{-1/2} \mathbf{d} - p}{\text{trace}\{\mathbf{R}^{-1/2} \mathbf{H} \mathbf{B}_e^b (\mathbf{R}^{-1/2} \mathbf{H})^T\}} \quad (5)$$

$$246 \mathbf{d} = \mathbf{y}^o - \mathbf{H} \bar{\mathbf{x}}^b \quad (6)$$

247 where \mathbf{d} is the observation innovation and p is the number of observations.



248 In order to reduce the influence of the spurious correlations on the performance of data assimilation, the EnKF was
249 performed locally in this study in that the analysis was calculated grid by grid with the assumption that only measurements
250 located within a certain distance (cutoff radius) from a grid point would influence the analysis results of this grid. The use of
251 this local analysis method also allowed the inflation factor to be calculated locally and to vary in time and space, which can
252 help characterize the spatiotemporal variations of errors. Similar to in Kong et al. (2021), the cutoff radius was chosen as 180
253 km for each species, and the same local scheme with a buffer area was employed to alleviate the discontinuities in the updated
254 state caused by the cut-off radius. A detailed description of the local analysis scheme is available in Kong et al. (2021). Table
255 1 then summarizes the corresponding relationships between the emissions and chemical concentrations. Similar to in Ma et al.
256 (2019) and Miyazaki et al. (2012), we did not consider the inter-species correlation during the assimilation, to prevent the
257 spurious correlations between non- or weakly related variables. In most cases, observations of one particular species were only
258 allowed to adjust the emissions of the same species. The assimilation of PM_{2.5} mass observation was more complicated than
259 that of other species as there are multiple error sources in the simulated mass concentrations of PM_{2.5}, not only from primary
260 emission, but also from secondary production. In this study, the PM_{2.5} mass observation was used to constrain the emissions
261 of PMF, BC and OC but not used to constrain the emissions of its precursors to avoid the spurious correlations and nonlinear
262 chemistry effects, which is similar to the scheme used in Ma et al. (2019). This is feasible since the emissions of primary PM_{2.5}
263 (i.e., PMF, BC and OC) and the emissions of PM_{2.5} precursors (e.g., SO₂, NO₂) were perturbed independently in our method,
264 thus the contributions of primary PM_{2.5} emission and the secondary PM_{2.5} productions to the PM_{2.5} mass could be isolated
265 through the use of ensemble simulations. Meanwhile, the use of iteration inversion method (which will be introduced later)
266 can further reduce the influence of the errors in the precursors' emissions on the inversion of primary PM_{2.5} emission, since
267 the precursors' emission would be constrained by their own observations during the iterations. However, the lack of
268 assimilation of speciated PM_{2.5} observations may lead to uncertainties in the estimated emissions of PMF, BC and OC, which
269 is a potential limitation in current work. To adjust the emissions of PMC, we used the observations of PM_{10-2.5} to avoid the
270 potential cross-correlations between PM_{2.5} and PM₁₀ (Peng et al., 2018; Ma et al., 2019). Due to the lack of long-term
271 nationwide NMVOC observations, the MDA8h O₃ was used to constrain the NMVOC emissions considering its strong
272 chemical relationship with the NMVOC emissions. Meanwhile, the use of MDA8h O₃ rather than the daily mean O₃
273 concentration could avoid the effects of the nighttime O₃ chemistry. Another important issue that should be noted when using
274 the MDA8h O₃ to constrain the NMVOC emission is that the errors in the simulation results of MDA8h O₃ are also caused by
275 the errors in NO_x emissions. The iteration inversion scheme could help deal with this issue as the errors in the NO_x emissions
276 will be constrained by the NO₂ observations in the next iteration, which can reduce the influences of errors in the NO_x emission
277 on the inversion of NMVOC emission based on the MDA8h O₃ concentrations. Meanwhile, although the O₃ concentration are
278 chemically related to the NO_x emissions, we did not use the O₃ concentrations to constrain the NO_x emission in this study since
279 there is nonlinear relationship between the O₃ concentration and NO_x emission which would lead to wrong adjustment of NO_x
280 emissions (Tang et al., 2016).

281 As we illustrated before, there exists nonlinear effects in the atmospheric chemistry which could influence the inversion
282 results of different species. In addition, since we did not consider the temporal variations in the *a priori* emissions, it was
283 expected that there would be significant biases in the *a priori* emissions for the years after 2013, as substantial changes in
284 emissions were expected owing to the implementation of strict emission control measures. Such bias in the *a priori* emissions
285 does not conform to the assumption of the EnKF that the *a priori* estimate is unbiased, which could thus lead to incomplete
286 adjustments of the *a priori* emissions and degrade the performance of the data assimilation (Dee and Da Silva, 1998). To
287 address these issues, an iteration inversion scheme was employed in this study, which has been used previously in Kong et al.
288 (2023). The main idea of the iteration inversion scheme is to preserve the background perturbation \mathbf{X}^b but to update the
289 ensemble mean of the state variable $\bar{\mathbf{x}}^b$ based on the inversion results of the *k*th iteration and corresponding model simulation.
290 The state variable used in the (*k* + 1)th inversions is formulated as follows:



$$x_i^{b,k+1} = [c^k + c_i^e - \bar{c}^e, \beta^k + \beta_i^e - \bar{\beta}^e]^T, \quad (7)$$

where c^k represents the model simulations using the inversed emissions of the k th iteration, c_i^e represents the i th member of ensemble simulations with an ensemble mean of \bar{c}^e , β^k represents the updated scaling factors at the k th iteration, and β_i^e represents the i th member of the ensemble of scaling factors with a mean value of $\bar{\beta}^e$. Two rounds of iteration were conducted in this study, which is enough for reducing the biases in the *a priori* emissions.

2.3.3 Setup of inversion estimation

Based on this inversion scheme, we firstly constrained the daily emissions of PMF, PMC, BC, OC, NO_x, SO₂, CO, and NMVOCs, from 2013 to 2020, based on the daily averaged observations of PM_{2.5}, PM_{10-2.5}, NO₂, CO, and MDA8h O₃. However, similar to in Kong et al. (2023), we only provide the emissions of PM_{2.5} (PMF+BC+OC) and PM₁₀ (PM_{2.5}+PMF) for the aerosol species since the lack of speciated PM_{2.5} observations would lead to uncertainties in the estimated emissions of PMF, BC, and OC as we mentioned before. Meanwhile, as mentioned in subsection 2.3.1, the meteorological and model uncertainty were not considered in the ensemble simulation. Thus, the errors in the meteorological simulation would cause fluctuations in the daily emissions that could contaminate the inversion results, which would be difficult to isolate from the inherent variations of emissions (Tang et al., 2013). Considering this, the daily emissions were averaged to monthly values to reduce the influences of random model errors after the assimilation.

3 Performance of the chemical data assimilation system

3.1 Analysis of OmF and emission increment

The observation-minus-forecast (OmF) and emission increment (*a posteriori* emission minus *a priori* emission) were firstly analyzed to demonstrate the performance of the data assimilation. As shown in Fig. 3, the *a priori* simulation generally underestimated the PM_{2.5} concentrations over the NCP, SE and SW regions (positive OmF values) during 2013–2014, but overestimated the PM_{2.5} concentrations from 2016, reflecting the effects of the emission control measures during these years. In the NE, NW and central China (hereafter, “Central”) regions, obvious underestimation of the PM_{2.5} concentration was found (positive OmF values) throughout almost the entire assimilation period. Similarly, the OmF values of PM₁₀ were positive throughout the whole assimilation period over all regions of China. In contrast, the OmF values for SO₂ were negative for most regions, and the negative OmF values over the NCP region became larger as the years progressed, which reflects the effects of the emission control measures. The OmF for NO₂ reveals a seasonal variation over the NCP and SE regions, with negative values during summer and positive values during winter, while there were obvious positive OmF values over the NE, SW, NW and Central regions. In terms of CO, large positive OmF values were found over all regions of China, and there were decreasing trends in the OmF values of CO over different regions of China associated with the emission control policies during these years. The OmF values for O₃ were positive over most regions of China, except the NW region. These results suggest that the *a priori* emissions may underestimate the emissions of PM_{2.5}, PM₁₀, CO, NO₂ and NMVOCs in China, but overestimate the SO₂ emissions. However, since our inversion method did not differentiate between anthropogenic and natural emissions, the biases in the model simulation may also be attributable to the errors in natural emissions such as dust, especially over the major dust-source areas of China (e.g., the NW and Central regions). In addition, the effects of emission control were not considered in the *a priori* emissions, which is another important contributor to the errors in the model simulation for the later years. Thus, the emission increments calculated by the assimilation should reflect the combined effects of errors in the anthropogenic and natural emissions, as well as the emission control.

The calculated emission increments were consistent with the OmF values for all species, which indicates that the data assimilation method can probably constrain the emissions based on the observations. According to Fig. 3, the emission increments were positive for PM_{2.5} over the NE, NW and Central regions, for NO₂ over the NE, SW, NW and Central regions,



331 and for PM₁₀, CO and NMVOC over almost all regions throughout the assimilation period. In contrast, the emission increments
332 were negative for the SO₂ emissions for most cases. Consistent with the OmF values, the emission increments were positive
333 for PM_{2.5} over the NCP, SE and SW regions during 2013–2014, but became negative from 2016 owing to the implementation
334 of strict emission control measures. The emission increments for NO_x also showed significant seasonal variation over the NCP
335 and SE regions, being positive during winter and negative during summer. The *a posteriori* biases for the model simulations
336 of different species were also plotted to assess the performance of the data assimilation. It can be clearly seen that the biases
337 were substantially reduced for all species, and the calculated root-mean-square error (RMSE) reduced by 23.2–52.8% for PM_{2.5},
338 19.9–37.8% for PM₁₀, 36.4–77.3% for SO₂, 18.3–25.2% for NO₂, 29.9–40.5% for CO, and 4.4–26.1% for O₃ over the different
339 regions of China, suggesting a good performance of the data assimilation system.

340 3.2 Evaluation of the inversion results

341 Table 2 shows the calculated evaluation statistics for the inversion at different temporal scales. It can be clearly seen that
342 the model simulation with the *a posteriori* emission inventory reproduced well the magnitude and temporal variations of the
343 different air pollutants in China, with calculated correlation coefficients of approximately 0.77, 0.72, 0.64, 0.67, 0.69 and 0.71,
344 and normalized mean biases of approximately 4.5%, –4.6%, –9.0%, –3.9%, –8.8% and 9.5%, for the hourly concentrations of
345 PM_{2.5}, PM₁₀, SO₂, NO₂, CO and O₃, respectively. Moreover, the *a posteriori* model simulation achieved comparable accuracy
346 with the air quality reanalysis data we developed in Kong et al. (2021) in terms of the RMSE, which was 32.4 μg·m⁻³, 53.1
347 μg·m⁻³, 24.9 μg·m⁻³, 19.9 μg·m⁻³, 0.56 mg·m⁻³ and 34.9 μg·m⁻³, respectively, for these species at the hourly scale. At the daily,
348 monthly and yearly scales, the constrained model simulation performed better, with RMSEs of about 9.1–20.0 μg·m⁻³ (PM_{2.5}),
349 18.5–31.6 μg·m⁻³ (PM₁₀), 11.5–16.0 μg·m⁻³ (SO₂), 8.1–12.8 μg·m⁻³ (NO₂), 0.28–0.39 mg·m⁻³ (CO), and 14.2–26.1 μg·m⁻³ (O₃),
350 which were respectively reduced by 56.7–67.3%, 49.2–52.1%, 68.8–72.8%, 36.3–39.8%, 47.0–58.0%, and 22.9–30.5%
351 compared to the RMSEs of the *a priori* simulations. These validation results confirm the good performance of the data
352 assimilation method and indicate that the inversed emissions inventory can reasonably represent the magnitude and long-term
353 trends of the air pollutant emissions in China during 2013–2020.

354 4 Results

355 Based on the top-down estimation, the gridded emissions for PM_{2.5}, PM₁₀, SO₂, CO, NO_x and NMVOCs over China from
356 2013 to 2020 were developed into what we have called the Inversed Emissions Inventory for Chinese Air Quality (CAQIEI).
357 In the following sections, we first analyze the magnitude and seasonality of the air pollutant emissions in China by taking 2015
358 as a reference year for when the number of observation sites became stable. After that, the changes in emissions of different
359 air pollutants are analyzed and compared between the two clean air action plans in China. Finally, CAQIEI is compared to the
360 previous bottom-up and top-down emission inventories to validate our top-down estimation and identify the potential
361 uncertainties in the current understanding of China's air pollutant emissions.

362 4.1 Top-down estimated Chinese air pollutant emissions in 2015

363 The top-down estimated emissions of different species in 2015 are as follows: 25.2 Tg of NO_x, 17.8 Tg of SO₂, 465.4 Tg
364 of CO, 15.0 Tg of PM_{2.5}, 40.1 Tg of PM₁₀, and 46.0 Tg of NMVOCs. Note that these values not only contain anthropogenic
365 emissions but also natural (e.g., dust and biogenic NMVOC) emissions. Thus, the top-down estimated emissions of PM and
366 NMVOCs were higher than those estimated by previous studies, as we mention in the following sections. Emission maps of
367 all species in 2015 are shown in Fig. 4, and the calculated emissions of different species over different regions are presented
368 in Table 3. According to Fig. 4, NCP was the region with the largest emission intensity of air pollutants in China, contributing



369 5.1 Tg of NO_x, 3.5 Tg of SO₂, 82.2 Tg of CO, 2.7 Tg of PM_{2.5}, 8.7 Tg of PM₁₀ and 9.0 Tg of NMVOCs to the total emissions
370 in China. There were also obvious emission hotspots distributed over the large cities of other regions, reflecting the influences
371 of human activities. In general, the majority of air pollutant emissions were located in eastern China (including the NCP, NE
372 and SE regions), where the economy is relatively well developed, which in total accounted for 66.0% of NO_x, 60.9% of SO₂,
373 57.5% of CO, 60.4% of PM_{2.5}, 60.5% of PM₁₀, and 67.8% of NMVOC emissions in China. However, although the GDP of
374 western China (including the SW, NW and Central regions) is less than one third that of eastern China, the top-down estimation
375 indicates that the air pollutant emissions in western China could have accounted for about 32.2–42.5% of the total emissions,
376 which reflects the low emission control levels over these regions.

377 Figure 5 shows the monthly variations of air pollutant emissions in China. The monthly profile of NO_x emissions was
378 relatively flat among the six species. SO₂ and CO showed higher emissions during wintertime because of the enhanced
379 residential emissions associated with higher coal consumption for heating during that time of year. Meanwhile, the emission
380 factor for CO from vehicles in winter was also higher than in other seasons, due to additional emissions from the cold-start
381 process (Kurokawa et al., 2013; Li et al., 2017b). PM_{2.5} and PM₁₀ had higher emissions during winter and spring, which, on
382 the one hand was due to the enhanced emissions from the residential and industrial sectors during wintertime (Li et al., 2017b),
383 whilst on the other hand was due to the enhanced dust emissions during the spring season (Fan et al., 2021). Emissions of
384 NMVOCs exhibited strong monthly variations, with higher emissions mainly in summer because of the enhanced NMVOC
385 emissions from biogenic sources.

386 4.2 Top-down estimated emission changes of different air pollutants

387 4.2.1 Emission changes of particular matter

388 Figure 6 shows the top-down estimated emission changes of PM_{2.5} and PM₁₀ over China during two clean air action
389 periods. Both PM_{2.5} and PM₁₀ emissions decreased substantially, by 44.3% and 21.2% respectively, from 2013 to 2020. On
390 the contrary, the top-down estimates showed increases of PM_{2.5} and PM₁₀ emissions in 2014 and 2015, but this would be likely
391 to be a spurious trend caused by the changes of observation sites as seen by the good correlation between the inversed PM_{2.5}
392 emissions and the observational coverage over the NW region (Fig. 2 and Fig. S1). Therefore, the emissions in 2013 and 2014
393 were discarded to prevent the spurious trends. According to Fig. 6, the PM_{2.5} emissions decreased by 14.5% during the 2013–
394 2017 clean air action period, from 15.0 Tg in 2015 to 12.8 Tg in 2017, and the reduction in emissions was roughly uniform
395 throughout the period, which was about 8% compared to previous years. The PM₁₀ emissions showed a smaller reduction rate
396 (–7.2%) than that of PM_{2.5}, decreasing from 40.1 Tg in 2015 to 37.2 Tg in 2017. Compared with the emission reduction rate
397 during the 2013–2017 action plan, both PM_{2.5} and PM₁₀ showed larger emission reduction rates during the 2018–2020 action
398 period, estimated to be 27.2% and 25.5%, respectively, from 2018 to 2020. The emission reductions in each year were also
399 larger, especially for PM₁₀. For example, PM_{2.5} and PM₁₀ emissions reduced by about 19.3% and 14.0% in 2019 compared to
400 2018. This may have been due to the strict controls imposed on the industrial and power sectors during the 2013–2017 action
401 period, along with the strengthened controls on residential emissions during the 2018–2020 action period. In particular, “coal-
402 to-electricity” and “coal-to-gas” strategies were vigorously implemented in northern China during wintertime to reduce coal
403 consumption and related air pollutant emissions (Liu et al., 2016; Wang et al., 2020a). Thus, our inversion results confirm the
404 effectiveness of the controls on residential emissions in terms of reducing the emissions of PM_{2.5} and PM₁₀. In addition, the
405 control of non-point sources, such as blowing-dust emissions, was also strengthened during the 2018–2020 action period,
406 which is consistent with the faster reduction of PM₁₀ emissions during 2018–2020. The annual trends of PM_{2.5} and PM₁₀
407 emissions were also calculated in China using the Mann–Kendall trend test and the Theil–Sen trend estimation method, the
408 results of which are summarized in Table 4. The calculation of emission trends can help extend the existing emission datasets
409 forward in time to produce up-to-date products. The top-down estimated trends of PM_{2.5} and PM₁₀ emissions were –1.4 and



410 -2.6 Tg/year during 2015–2020, attributable to the strict emission control measures imposed during the two clean air action
411 plans. As mentioned, the decreasing trends were larger during the 2018–2020 action plan (-1.5 and -4.6 Tg/year) than during
412 the 2013–2017 action plan (-1.1 and -1.5 Tg/year).

413 On the regional scale (Fig. S1), it can be clearly seen that the $PM_{2.5}$ emissions decreased consistently over all regions, by
414 59.8% in NCP, 49.6% in SE, 39.5% in NE, 35.8% in SW, 33.2% in NW, and 41.0% in Central, from 2015 to 2020. The NCP
415 region showed the largest reduction in emissions among the six regions, with its emission reduction rate being almost larger
416 than 10% in each year. This is consistent with the strictest emission control policies having been imposed over the NCP region.
417 The SE region showed a similar reduction in emissions to the NCP region, with its emission reduction rate being larger than
418 10% in most years. Obvious increases of $PM_{2.5}$ emissions could be found over the NW region from 2013 to 2015 possibly
419 owing to the increase in the number of observation sites in those years. After 2015, $PM_{2.5}$ emissions generally decreased over
420 the NW region, while there was a slight rebound in $PM_{2.5}$ emissions in 2016 and 2018, possibly due to the influences of the
421 errors in fine dust emission. The Central region showed different characteristics of emission changes to the other regions
422 insofar as it showed little change in $PM_{2.5}$ emissions during 2015–2018 but large reductions in 2019. This may be consistent
423 with the control of emissions over the Fengwei Plain area (the part of the Central region where the emission intensity is largest)
424 being weak during the 2013–2017 action plan but strengthened during the 2018–2020 action plan. In terms of the $PM_{2.5}$
425 emission trends over the different regions, the calculated $PM_{2.5}$ emission trends were about -0.32 Tg/year in NCP, -0.32
426 Tg/year in SE, -0.24 Tg/year in NE, -0.21 Tg/year in SW, -0.09 Tg/year in NW, and -0.15 Tg/year in Central, from 2015 to
427 2020.

428 The changes of PM_{10} emissions were generally similar to those of $PM_{2.5}$, i.e., with decreases in all regions from 2015 to
429 2020 (Fig. S2). The top-down estimated PM_{10} emission reductions from 2015 to 2020 were about 3.5 Tg (40.0%) in NCP, 2.6
430 Tg (35.5%) in SE, 3.0 Tg (36.6%) in NE, 2.0 Tg (35.9%) in SW, 1.0 Tg (25.3%) in NW, and 1.3 Tg (21.6%) in Central; and
431 the calculated trends were about -0.64 Tg/yr, -0.52 Tg/yr, -0.51 Tg/yr, -0.40 Tg/yr, -0.20 Tg/yr, and -0.27 Tg/yr,
432 respectively. However, due to the influences of the changes in the number of observation sites, the PM_{10} emissions over the
433 NE, SW and NW regions increased substantially from 2013 to 2015, while they decreased in almost all years after 2015.
434 Different from the other regions, the Central region showed increases in PM_{10} emissions from 2015 to 2018, by about 0.92 Tg
435 (14.9%), but substantial decreases in 2019 and 2020. This also shows that most PM_{10} emission reductions were achieved during
436 the 2018–2020 action plan. According to CAQIEI, the PM_{10} emissions decreased by 0.64–2.3 Tg (17.4–31.8%) from 2018 to
437 2020, which accounted for 48.4–169.0% of the total reduction in emissions from 2015 to 2020. This again emphasizes the
438 effectiveness of the control of blowing-dust emissions during the 2018–2020 action plan.

439 4.2.2 Emission changes of gaseous air pollutants

440 4.2.2.1 SO_2 and CO

441 Figure 7 shows the emission changes of different gaseous air pollutants in China from 2013 to 2020. Similar to the PM
442 emissions, SO_2 and CO emissions decreased continuously during the two action plan periods, with top-down estimated
443 emission reductions of about 9.6 Tg (54.1%) and 166.3 Tg (35.7%) for SO_2 and CO from 2015 to 2020, respectively.
444 Meanwhile, both SO_2 and CO showed a significant decreasing trend from 2015 to 2020, with estimated trends of approximately
445 -2.1 Tg/yr and -36.0 Tg/yr, respectively (Table 5). The reductions in SO_2 and CO emissions are closely consistent with the
446 strict emission control measures imposed during the action plan periods, such as the phasing out of outdated industrial capacity
447 and high-emitting factories, the strengthening of emission standards for industry and the power sector, the elimination of small
448 coal-fired industrial boilers, and the replacement of coal with cleaner energies, which reflects the effectiveness of the emission
449 control measures during the two action plan periods. Reductions of SO_2 emission were generally steady during the two action
450 plan periods, which were approximately 4.2 Tg (23.8%) from 2015 to 2017 and 2.5 Tg (23.5%) from 2018 to 2020. However,
451 CO showed a different emission reduction rate during the two action plan periods, with its emission reductions (67.1 Tg, 18.3%)



452 during the 2018–2020 action plan being larger than those (45.6 Tg, 9.8%) during the 2013–2017 action plan. This contrast
453 reflects the different emission control policies during the two clean air action periods, as well as the different emission
454 distributions among the sectors between SO₂ and CO. According to the estimates of Zheng et al. (2018), the share of emissions
455 from the industrial and power sector for SO₂ (77%) is nearly double that for CO (39%). Thus, the smaller reduction of CO
456 emissions during the 2013–2017 action plan than that of SO₂ provides evidence that the 2013–2017 action plan mainly focused
457 on controlling the emissions from the industrial and power sectors. During the 2018–2020 action plan, strict control measures
458 targeted on the residential and transportation sectors were also implemented, which together account for 61% of CO emissions
459 but only 23% of SO₂ emissions. As a result, CO showed a larger emission reduction rate during the 2018–2020 action plan,
460 while the emission reduction rate for SO₂ was similar to that in the 2013–2017 action plan. The calculated trends of SO₂ and
461 CO emissions during the two action plans are presented in Table 4, which are –2.1 Tg/yr and –1.3 Tg/yr for SO₂, and –22.8
462 Tg/yr and –33.5 Tg/yr for CO, respectively.

463 The reduction of SO₂ and CO emissions was also evident on the regional scale (Fig. S3 and S4). According to the top-
464 down estimation, the reduction of SO₂ emissions ranged from 0.44 to 2.42 Tg (41.7–69.9%) from 2015 to 2020, with the NCP
465 region exhibiting the largest reductions. The calculated decreasing trend of SO₂ emissions was also significant over all regions,
466 ranging from –0.08 Tg/yr over the NW region to –0.57 Tg/yr over the NCP region (Table 5). With regards to the emission
467 reduction rate during the different action plans, the results suggest that the emission reduction rate of SO₂ was higher during
468 the 2013–2017 action plan (by 20.8–39.8%) than that during the 2018–2020 action plan (16.6–29.0%) over the NCP, SE, NE
469 and SW regions. This may have been because, after the strict emission controls imposed upon industry and power plants during
470 the 2013–2017 action plan, the room for further reductions in SO₂ emissions become smaller during the 2018–2020 action
471 plan over these regions. Although residential and vehicle emissions were controlled more strictly during the 2018–2020 action
472 plan, in total they account for ~20% of anthropogenic SO₂ emissions in China (Zheng et al., 2018). Thus, the enhanced
473 reductions in SO₂ emissions from the residential and transportation sectors may not have been able to fully compensate for the
474 weakened reductions from the industrial and power sectors, leading to a smaller SO₂ emission reduction rate over these regions.
475 In contrast, the SO₂ emission reduction rate during the 2018–2020 action plan (31.1–34.8%) was higher than that during the
476 2013–2017 action plan (14.1–20.4%) over the NW and Central regions. This may have been due to the fact that the emission
477 controls over the NW and Central regions were relatively weak during the 2013–2017 action plan (as also evidenced by the
478 emission reduction rates of other species) owing to its less-developed economy. During the 2018–2020 action plan, the
479 emission controls over these two regions were strengthened, which led to their higher emission reduction rates. Accordingly,
480 the enhanced SO₂ emission reduction rates over the NW and Central regions compensated for the weakened reduction rates
481 over the other regions, leading to a steady SO₂ emission reduction rate on the national scale.

482 The reductions of CO emissions from 2015 to 2020 were approximately 14.9–42.3 Tg (21.6–51.4%) over the different
483 regions of China, with significant decreasing trends ranging from –3.0 to –8.7 Tg/yr (Fig. S3 and Table 5). Consistent with
484 the comparisons of national CO emission reduction rates between the two action plans, the emission reduction rates during the
485 2013–2017 action plan (4.4–24.6%) were estimated to be smaller than those during the 2018–2020 action plan (12.2–24.6%)
486 over all the different regions except the Central region, where the CO emission reduction rate was similar during the two action
487 plans (Fig. S4).

488 4.2.2.2 NO_x and NMVOCs

489 The top-down estimated NO_x and NMVOC emissions showed different changes to the other four species, by increasing
490 during the 2013–2017 action plan but declining during the 2018–2020 action plan. Specifically, NO_x emissions increased
491 slightly by 5.9% from 2015 (25.2 Tg) to 2017 (26.6 Tg), with a non-significant increasing trend of 0.74 Tg/yr. Then, NO_x
492 emissions began to decrease in 2018, with a top-down estimated emission reduction and calculated trend of approximately 3.1
493 Tg (12.7%) and –1.6 Tg/yr, respectively, from 2018 to 2020. NMVOCs showed stronger emission increases than did NO_x,



494 with top-down estimated emission increases of approximately 12.7 Tg (27.6%) and a calculated emission trend of about 6.3
495 Tg/yr from 2015 to 2017. Similar to NO_x, NMVOC emissions began to decrease after 2018, with a top-down estimated
496 reduction of approximately 2.6 Tg (−4.4%) from 2018 to 2020, and a calculated trend of about −1.3 Tg/yr.

497 The increases of NO_x and NMVOC emissions indicate that the 2013–2017 action plan may not have achieved desirable
498 mitigation effects on these two species. For NO_x emissions, the upward trend may have been associated with the following
499 three factors. Firstly, vehicle exhaust is one of the most important sources of NO_x in China, accounting for 31% of all NO_x
500 emissions nationally (Zheng et al., 2018). From 2013 to 2017, the number of vehicles in China continued to increase and
501 reached 310 million in 2017, approximately 33.5% higher than in 2013 (MEE, 2017), which led to increases of NO_x emissions
502 from vehicles in China. Secondly, as discussed, the control measures implemented during the 2013–2017 action plan mainly
503 focused on power plants and industrial sources. Controls on vehicle sources were relatively weak. In particular, vehicles with
504 high NO_x emissions, such as heavy-duty diesel trucks, were not controlled strictly during the 2013–2017 action plan. Thirdly,
505 although the 2013–2017 action plan was effective in reducing the NO_x emissions from coal-fired power plants by promoting
506 denitrification facilities and an ultra-low emission standard, the mitigation impacts on industrial NO_x emissions may have been
507 relatively small. For example, Wang et al. (2019a) compiled a unit-based emissions inventory for China’s iron and steel
508 industry from 2010 to 2015, based on detailed survey results of approximately 4900 production facilities in mainland China.
509 They found that there were almost no NO_x control measures in China’s iron and steel industry during 2010–2015, resulting in
510 a 12.4% increase in China’s NO_x emissions from the iron and steel industry in 2015 compared to 2010. In addition, although
511 the penetration rate of denitrification facilities in China’s cement industry reached 92% in 2015, the actual operating rate of
512 denitrification facilities in the cement industry was not desirable, due to the lack of online emission monitoring systems.
513 According to the research results of the Ministry of Ecology and Environment, 800, 1300, and 1400 cement production kilns
514 were equipped with selective non-catalytic denitrification facilities from 2013 to 2015, but the actual operating rates were only
515 51%, 54% and 73%, respectively (Liu et al., 2021). In addition, the new precalciner kilns used in the cement industry have a
516 higher NO_x emission factor, such that the shift from traditional vertical kilns to precalciner kilns has to some extent increased
517 the cement industry’s emissions of NO_x (Liu et al., 2021). Thus, there is evidence that the mitigation effects of the industrial
518 control measures on NO_x emissions may not be as significant as expected. Overall, the increased number of vehicles may have
519 offset the emission mitigation effects brought about by the control of power plants. Meanwhile, the mitigation effects of
520 controlling vehicle and industrial NO_x emissions were undesirable. Consequently, NO_x emissions in China may not have
521 decreased, and even increased slightly, during the 2013–2017 action plan. Figure S5 further shows the changes in NO_x
522 emissions over different regions of China, revealing that NO_x emissions over the NCP, SE, NE and SW regions were roughly
523 unchanged (by less than 5%) from 2015 to 2017, while they increased over NW (18.6%) and Central (17.5%). This is consistent
524 with previous results and indicates that NO_x emissions may have increased over the NW and Central regions, possibly due to
525 their increased human activities and weak emission controls.

526 In terms of NMVOC emissions, since the inversion results did not differentiate between anthropogenic and biogenic
527 sources, the changes in NMVOC emissions may have been related to both anthropogenic and biogenic emissions. With respect
528 to anthropogenic emissions, previous bottom-up studies have suggested that China’s NMVOC emissions did not decline during
529 the 2013–2017 action plan, due to the lack of effective control measures on the chemical industry and solvent use (Zheng et
530 al., 2018; Li et al., 2019c). According to the estimates of Li et al. (2019c), China’s NMVOC emissions from solvent use
531 increased by 11.1% in 2017 compared to those in 2015. Meanwhile, the increase in the number of vehicles in China may also
532 have led to an increase in NMVOC emissions from transportation. According to the estimations of Li et al. (2020a), there was
533 also an upward trend in China’s biogenic NMVOC emissions from 2008 to 2018 because of the increased vegetation cover
534 and air temperature. Compared to the emissions in 2008, China’s biogenic NMVOC emissions increased by 20.18% in 2017,
535 with an average annual rate of increase of 2.03%. Therefore, the increases in NMVOC emissions from the chemical industry,
536 solvent use, and vehicles, together with the increase in biogenic NMVOC emissions, may be the main reasons for the increased



537 NMVOC emissions during the 2013–2017 action plan. Figure S6 further shows the changes in NMVOC emissions over
538 different regions of China, which suggests consistent increases in NMVOC emissions from 2015 to 2017 over different regions.
539 According to the top-down estimations, NMVOC emissions increased by 30.5%, 25.2%, 18.5%, 10.9%, 50.5% and 63.1%
540 over the NCP, SE, NE, SW, NW and Central regions, respectively. Again, the NW and Central regions exhibited the largest
541 emission increases among the six regions, which is consistent with their elevated levels of human activity and weak emission
542 controls.

543 The decrease in NO_x and NMVOC emissions after 2018 suggests that the emission control strategy of the Chinese
544 government had reached a point of optimization. The 2018–2020 action plan not only strengthened the controls over the
545 industrial and power sectors, but also the transportation sector, especially for diesel vehicles with high NO_x emissions. For
546 example, the Chinese government released the “Action Plan for the Control of Diesel Trucks”, and vigorously promoted an
547 adjustment of the transportation structure of China by gradually improving the availability of rail transport. As a result, there
548 was a downward trend in NO_x emissions in China. The top-down estimated reductions of NO_x emissions were approximately
549 0.81 Tg (17.2%) over NCP, 0.98 Tg (14.0%) over SE, 0.37 Tg (9.4%) over NE, 0.51 Tg (12.2%) over SW, 0.13 Tg (11.0%)
550 over NW, and 0.32 Tg (9.2%) over Central (Fig. S5). The decrease in NMVOC emissions after 2018 may on the one hand
551 have been related to the strengthening of vehicle controls during the 2018–2020 action plan, whilst on the other hand it may
552 have been related to the promotion of clean heating plans in the northern region, which reduced the emissions of NMVOCs
553 from residential sources. However, the decreases in NMVOC emissions were smaller than those in NO_x , which were estimated
554 to be 0.84 Tg (6.9%) over NCP, 0.47 Tg (2.8%) over SE, 0.98 Tg (10.1%) over NE, and 0.53 Tg (14.1%) over NW (Fig. S6).
555 Different from other regions, the NMVOC emissions over the SW and Central regions remained almost unchanged during the
556 2018–2020 action plan (Fig. S6).

557 4.2.3 Changes in the distribution pattern of emissions in China

558 Due to the different emission control intensities over the different regions of China, the emission distribution patterns of
559 the different species may also have been altered, which could have influenced the distributions of air pollution in China. Based
560 on CAQIEI, we further investigated the emission distribution patterns, as well as their changes, during the two action plans.
561 Maps of the emission changes of different species during the 2013–2017 action plan and the 2018–2020 action plan are
562 presented in Fig. 8. The shares of emissions in 2015, 2017 and 2020 by each subregion of China are also presented (Fig. 9). It
563 can be seen that the emission changes during the 2013–2017 action plan were more heterogenous than those during the 2018–
564 2020 action plan. The air pollutant emissions after the 2018–2020 action plan showed consistent reductions over most regions
565 of China, while there were obvious emission increases detected over the 2013–2017 action plan. This is consistent with the
566 different emission control efficiencies during the two clean air action plans as mentioned in previous sections. Due to its
567 strictest emission control policies, the NCP region showed consistent emission reductions of SO_2 , NO_x , CO, $\text{PM}_{2.5}$ and PM_{10}
568 during the two clean air action plans. Accordingly, the shares of emissions in the NCP region continued to decrease during the
569 two action plan periods (Fig. 9). For example, the share of SO_2 emissions in the NCP region decreased from 19.4% to 15.4%
570 after the 2013–2017 action plan, and from 15.4% to 12.7% after the 2018–2020 action plan. In contrast, NMVOC emissions
571 increased obviously over the NCP region during the 2013–2017 action plan, and decreased during the 2018–2020 action plan.
572 However, its share did not change significantly during the two action plans, being roughly 20% throughout both periods. As
573 for other regions, increases of SO_2 , NO_x , $\text{PM}_{2.5}$, PM_{10} and NMVOC emissions during the 2013–2017 action plan could be
574 found over the Central region. More specifically, the emission increases were mainly located in the Fenwei Plain area of the
575 Central region, which was due to the fact that this area was not included as a key region of emission controls during the 2013–
576 2017 action plan. However, the Fenwei Plain area was added as a key emission control region during the 2018–2020 action
577 plan, which is consistent with the emission reductions for these species over the Central region (Fig. 8). As a result, the shares
578 of SO_2 and $\text{PM}_{2.5}$ emissions in the Central region increased in the 2013–2017 action plan but decreased in the 2018–2020



579 action plan (Fig. 9). However, the shares of NO_x , PM_{10} and NMVOC emissions continued to increase over the Central region
580 during the two clean air action plans, which suggests larger roles of air pollutant emissions in that region. In contrast, the share
581 of CO emissions in the Central region continued to decrease in the two action plans, from 17.7% in 2015 to 13.4% in 2020. In
582 terms of the shares of emissions in eastern and western China, the top-down estimation suggests an increased share of NO_x ,
583 $\text{PM}_{2.5}$, PM_{10} and NMVOC emissions in western China after the two clean air action plans (Fig. 9), which indicates slower
584 emission reductions for these species in western China. However, the share of CO emissions in western China was reduced
585 after the two clean air action plans. Although the share of SO_2 emissions in western China increased during the 2013–2017
586 action plan, it turned to a decrease in the 2018–2020 action plan.

587 4.3 Comparisons with different bottom-up emission inventories

588 4.3.1 Magnitude

589 In this subsection, we compare CAQIEI with previous long-term bottom-up and top-down emission inventories in China
590 to validate our inversion results and identify the potential uncertainty in the current understanding of China's air pollutant
591 emissions. The emission inventories adopted were MEIC (Zheng et al., 2018), ABaCAS (Li et al., 2023), HTAPv3 (Crippa et
592 al., 2023), EDGARv6 (Jalkanen et al., 2012), CEDS (McDuffie et al., 2020), and the top-down emission estimates from the
593 updated Tropospheric Chemistry Reanalysis (TCR-2) (Miyazaki et al., 2020b). Since the latest year of most emission
594 inventories is 2018, the comparisons were conducted between 2015 and 2018. In particular, the comparison with MEIC is
595 highlighted considering its wide application in Chinese air pollution studies. Considering that the top-down estimation includes
596 both anthropogenic and natural sources, the natural emission sources, including soil NO_x emissions and biogenic emissions
597 obtained from the CAMS global emission inventory ([https://ads.atmosphere.copernicus.eu/cdsapp#!/dataset/cams-global-](https://ads.atmosphere.copernicus.eu/cdsapp#!/dataset/cams-global-emission-inventories?tab=overview)
598 [emission-inventories?tab=overview](https://ads.atmosphere.copernicus.eu/cdsapp#!/dataset/cams-global-emission-inventories?tab=overview); last accessed 26 July 2023) and the biomass burning emissions obtained from the Global
599 Fire Assimilation System (GFAS) (Kaiser et al., 2012), were also analyzed to help explain the discrepancies between our
600 inversion results and previous inventories.

601 4.3.1.1 NO_x

602 Figure 10 shows the average emissions of different air pollutants in China during 2015–2018 obtained from CAQIEI and
603 the previous emission inventories plus natural sources. Comparisons of the emission estimations on the regional scale are also
604 presented (Fig. 11). The results show that CAQIEI has slightly higher NO_x emissions in China than the other inventories.
605 Considering that CAQIEI includes both anthropogenic and natural sources, this discrepancy could be explained by the natural
606 NO_x sources. According to the estimations of CAMS and GFAS, the soil and biomass-burning NO_x emissions are
607 approximately 1.9 and 0.08 Tg/yr, which explains well the higher NO_x emissions given by CAQIEI. After consideration of the
608 natural sources, MEIC, HTAPv3 and EDGARv6 agree well with our inversion results on the national scale, with their
609 differences within 1.0–7.4%. This confirms well our inversion results and suggests that there is no significant bias in the
610 estimations of total NO_x emissions in China for these inventories. ABaCAS, CEDS and TCR-2 may have low bias in their
611 estimated NO_x emissions considering their smaller values than CAQIEI and other emission inventories. However, the
612 differences between CAQIEI and these inventories were found to range from 15.9% to 21.3%, which is consistent with
613 previous estimated uncertainties of NO_x emissions in China (Kurokawa and Ohara, 2020; Li et al., 2017b; Li et al., 2023). On
614 the regional scale, the top-down estimated NO_x emissions show good agreement with the previous emission inventories over
615 the NCP and SE regions, with their differences ranging from 1.0%–26.8%, suggesting lower uncertainties in the estimations
616 of NO_x emissions over these two regions. This makes sense because NCP and SE are the two most developed regions in China,
617 and where surveys and research on emissions are most sufficient. The uncertainties are larger over the other regions. In the NE
618 region, CAQIEI has higher NO_x emissions than the other inventories, by 5–70%. MEIC, CEDS and TRC-2 are closer to our



619 estimates, with their differences being approximately 5.4–23.3%, while the differences are larger for ABaCAS, HTAPv3 and
620 EDGARv6 (36.7–70.0%). This suggests that anthropogenic or biomass-burning emissions may be underestimated over the NE
621 region. Over the SW and Central regions, CAQIEI is higher than MEIC, ABaCAS, CEDS and TCR-2 by 29.4–40.8% and
622 22.4–47.4%, respectively, but is lower than HTAPv3 and EDGARv6 by about 30%, suggesting higher uncertainties of
623 estimated NO_x emissions over these two regions. In the NW region, CAQIEI is consistently higher than the previous inventories,
624 by 22.7–64.2%, which suggests a significant low bias may exist in current estimations of NO_x emissions over this region.

625 4.3.1.2 SO_2

626 For SO_2 emissions, since natural sources contribute little (only about 0.02 Tg/yr) to them in China, the discrepancies
627 between CAQIEI and previous emission inventories are mainly attributable to the differences in anthropogenic emissions. As
628 shown in Fig. 10, CAQIEI agrees well with HTAPv3 and CEDS on the national scale, with their differences being
629 approximately $\pm 2\%$, but is higher than MEIC, ABaCAS and TCR-2 by 17.4–32.9%, suggesting a negative bias in their
630 estimated SO_2 emissions in China. In contrast, EDGARv6 may have a positive bias in its estimated SO_2 emissions, which are
631 roughly double those of CAQIEI and other inventories. On the regional scale, our results agree well with MEIC, ABaCAS,
632 HTAPv3, CEDS and TCR-2 over the NCP region, with their differences ranging from 1.0 to 18.1%, suggesting lower
633 uncertainties in SO_2 emissions over this region. In the SE region, CAQIEI is lower than previous emission inventories, except
634 TCR-2. The differences are relatively smaller (by around -15%) for the MEIC and ABaCAS inventories, but larger for
635 HTAPv3, EDGARv6 and CEDS (ranging from -47.3% to -113.2%). This suggests that current global emission inventories
636 may overestimate the SO_2 emissions in the SE region. In contrast, CAQIEI is higher than all previous emission inventories
637 over the NE region by about 14.8–132.0%, which suggests a consistent negative bias may exist in current estimations of SO_2
638 emissions over this region. Similarly, CAQIEI is higher than MEIC, ABaCAS, CEDS and TCR-2, by 27.0–75.6%, in the NW
639 region, and by 44.3–77.7% in the Central region, suggesting a negative bias in estimations of SO_2 emissions over these two
640 regions. The SO_2 emissions estimated by HTAPv3 are closer to our inversion results, with their differences being about 6.9–
641 12.6%.

642 4.3.1.3 CO

643 For CO emissions, CAQIEI is substantially higher than the previous emission inventories, with the estimated CO
644 emissions of CAQIEI being about three times higher than the bottom-up inventories and more than double those of the top-
645 down estimates made by TCR-2. According to GFAS, the average rate of CO biomass-burning emissions in China from 2015
646 to 2018 was about 3.4 Tg/yr. Yin et al. (2019), based on MODIS fire radiative energy data, also estimated China's CO biomass-
647 burning emissions to be about 5.0 (2.3–7.8) Tg/yr. The biogenic CO emissions obtained from the CAMS global emission
648 inventory were approximately 2.3 Tg/yr. According to these estimates, natural CO emissions in China have a magnitude of
649 about 10^1 , which is rather small compared with anthropogenic sources, and cannot explain the large discrepancies between
650 CAQIEI and other inventories. Thus, there may be a large negative bias in current estimations of anthropogenic CO emissions
651 in China. In fact, the underestimation of CO anthropogenic emissions has been revealed in previous studies and is regarded as
652 the main reason for the negative bias in global or hemispheric CO simulations (Stein et al., 2014; Gaubert et al., 2020).
653 Regionally, Kong et al. (2020) compared a suite of 13 modeling results from six different CTMs—namely, NAQPMS, CMAQ,
654 WRF-Chem, NU-WRF, NHM-Chem and GEOS-Chem—with observations over the NCP and Pearl River Delta regions under
655 the framework of the Model Inter-Comparison Study for Asia III (MICS-Asia III), and found consistent negative biases in the
656 CO simulations of all models, pointing toward potential underestimations of CO emissions in China. Previous inversion studies
657 have also reported a significant underestimation of CO emissions in their *a priori* emission inventories (Bergamaschi et al.,
658 2000; Miyazaki et al., 2012; Petron et al., 2002; Petron et al., 2004; Tang et al., 2013; Gaubert et al., 2020). For example, the
659 inversion results reported by Gaubert et al. (2020) suggested that CEDS underestimates CO emissions by 80% in northern



660 China. Therefore, our inversion results are consistent with previous studies, which supports the point on the underestimation
661 of anthropogenic CO emissions in China. However, direct evidence in support of such high CO emissions in China is still
662 limited currently. Thus, we compiled more inversion results within the period of 2013–2020 from previous studies to further
663 validate our inversion results, which are summarized in Table 6. It can be clearly seen that there are large differences in the
664 estimated CO emissions between the inversion results based on surface observations and those based on satellite data. Our
665 inversion results are consistent with the results of Feng et al. (2020), with China's CO emissions in December 2017 estimated
666 at approximately 1500.0 kt/day and 1388.1 kt/day, respectively. In addition, Feng et al. (2020) used the CMAQ model to
667 constrain CO emissions, which is different from the model we used. This may indicate that the model uncertainty would not
668 significantly influence the inversion results of CO emissions. However, the top-down estimated CO emissions based on
669 satellite data (163.6–553.4 kt/day) are much lower than those based on surface observations, although they are all higher than
670 their *a priori* emissions. The lower CO emission estimations based on satellite data assimilation may be attributable to the
671 lower sensitivities of satellite data to surface concentrations, suggesting that the assimilation of satellite data alone may not be
672 adequate to correct the negative biases in the *a priori* emissions. This deficiency has also been revealed by Miyazaki et al.
673 (2020b), who found undercorrected surface CO emissions in the extratropics of the Northern Hemisphere in TCR-2. However,
674 the assimilation of surface observations can be influenced by the uncertainties in the modeled vertical mixing, which could
675 lead to the uncertainties in the inversed CO emissions based on surface observations. Therefore, the inversed CO emissions in
676 CAQIEI could be partly supported by previous inversion studies based on surface observations, but more evidence is still
677 needed to justify the magnitude of the inversed CO emissions. Besides anthropogenic sources, the chemical production of CO
678 via oxidation of methane (CH₄) and NMVOCs, as well as the CO sinks via the hydroxyl radical (OH) reaction, also influence
679 the simulation of CO (Stein et al., 2014; Gaubert et al., 2020; Müller et al., 2018). Due to the important role of OH in the
680 chemical production and sinks of CO, the inversion of CO emissions is sensitive to the modeled OH abundance and the
681 emissions of CH₄ and NMVOCs. According to the estimation of Müller et al. (2018), the magnitude of inversed CO emissions
682 in China could differ by more than 40% when different levels of OH concentrations are used in the model. Thus, the much
683 higher estimations of CO emissions in our inversion results may also be partly explained by the underestimation of CO
684 chemical production or the overestimation of the CO sink.

685 4.3.1.4 PM_{2.5}

686 In terms of PM_{2.5}, CAQIEI is about 20% higher than ABA-CAS, HTAPv3 and EDGARv6, and 47.7% higher than MEIC
687 on the national scale, suggesting that anthropogenic, biomass-burning, and/or fine-dust emissions may be underestimated.
688 Larger underestimations mainly occur in the NE and NW regions, where CAQIEI is about 27.2–114.9% and 83.2–143.2%
689 higher than the previous inventories. The underestimated PM_{2.5} emissions may be related to the underestimations of biomass-
690 burning or anthropogenic sources in the NE region (Wu et al., 2020b), while in the NW region, besides the possible
691 underestimation of anthropogenic sources as seen from the other species, the underestimated fine-dust emissions may also
692 contribute to the underestimation of PM_{2.5} emissions there. The differences in the estimated PM_{2.5} emissions are relatively
693 smaller in the NCP and SE regions, ranging from –18.9% to 20.4%, which shows better agreement in the estimated PM_{2.5}
694 emissions over these two regions. This confirms our inversion results and indicates lower uncertainty in the estimated PM_{2.5}
695 emissions over the NCP and SE regions. In the SW region, CAQIEI is closer to HTAPv3 and EDGARv6, with their differences
696 being about 6.3% and –9.5% respectively, and is higher than MEIC and ABA-CAS by 54.2% and 28.6%.

697 4.3.1.5 PM₁₀

698 For PM₁₀ emissions, it is difficult to directly compare CAQIEI with previous emission inventories since CAQIEI not only
699 contains anthropogenic and biomass-burning emissions, but also coarse-dust emissions. As a result, the estimated emissions
700 of PM₁₀ by CAQIEI are substantially higher than those by previous inventories, especially over the NW, Central and NE



701 regions (Fig. 11), which are the typical natural windblown dust-source regions in China (Zeng et al., 2020). Besides the
702 naturally windblown dust of arid desert regions (Prospero et al., 2002), large amounts of coarse-dust emissions also stem from
703 anthropogenic sources, including anthropogenic fugitive, combustion and industrial dust from urban sources (AFCID) (Philip
704 et al., 2017), and anthropogenic windblown dust from human-disturbed soils due to changes in land-use practices, deforestation
705 and agriculture (Tegen et al., 1996). Therefore, although the other regions are not typical natural windblown dust-source
706 regions in China, there are still high levels of coarse-dust emissions from anthropogenic sources there (also called “urban
707 dust”). The differences between CAQIEI and previous inventories over these regions may reflect the underestimated and/or
708 the unconsidered urban dust in previous emission inventories. Although AFCID is included in MEIC, ABaCAS, HTAPv3 and
709 EDGARv6, it is difficult for current bottom-up emission inventories to completely represent fugitive sources (Philip et al.,
710 2017). In addition, anthropogenic windblown dust emissions are not included in current bottom-up emission inventories, which
711 is an important source of coarse dust in urban areas according to the estimations of Li et al. (2016). Besides, similar to the
712 situation with PM_{2.5} emissions, anthropogenic and biomass-burning emissions may also be underestimated for PM₁₀ emissions,
713 which could partly explain the large differences between CAQIEI and previous inventories.

714 4.3.1.6 NMVOCs

715 For NMVOC emissions, since CAQIEI includes both anthropogenic and natural sources, its estimated NMVOC emissions
716 are much higher than those estimated by previous emission inventories. After consideration of natural sources, CAQIEI agrees
717 well with the MEIC, HTAPv3 and CEDS inventories on the national scale, with their differences being about 1.5–12.5%,
718 which validates our inversion results and the estimated NMNOV emissions for these inventories. ABaCAS and EDGARv6
719 may have a negative bias in their estimated NMVOC emissions, which are lower than CAQIEI by 17.8% and 24.6%,
720 respectively. On the regional scale, the comparison of CAQIEI with previous inventories suggests that there may be higher
721 NMVOC emissions over northern China (NCP, NE and NW). The top-down estimated NMVOC emissions are about 30.4–
722 81.4%, 27.3–72.1%, 79.3–116.8%, and 8.7–57.5% higher than those of the previous emission inventories over these regions.
723 This suggests that NMVOC emissions may be underestimated in northern China, especially over the Central region. In contrast,
724 the NMVOC emissions over the SE region may be overestimated, with the estimated NMVOC emissions of CAQIEI being
725 about 21.2–27.6% lower than those of MEIC, ABaCAS, HTAPv3 and CEDS. Over the SW region, CAQIEI shows good
726 agreement with MEIC, ABaCAS and CEDS, with CAQIEI being slightly lower than these inventories by 1.0–8.9%. HTAPv3
727 and EDGARv6 may overestimate the NMVOC emissions over the SW region, with their results being about 38.6% and 29.1%
728 higher than those of CAQIEI.

729 4.3.2 Seasonality

730 Figure 12 presents the monthly profiles of different air pollutants obtained from different emission inventories. Note that
731 the natural sources have been added to the previous inventories to facilitate the comparisons. The results show that different
732 emission inventories give similar monthly profiles of NO_x and CO emissions, with higher emissions during wintertime and
733 lower emissions during summertime, which suggests relatively lower uncertainty in the estimated monthly profiles for these
734 two species. For SO₂ emissions, CAQIEI yields stronger monthly variation than the other inventories, with a higher proportion
735 from January to March and lower proportion during summertime. Due to the influences of dust emissions, the top-down
736 estimated PM_{2.5} and PM₁₀ emissions show higher proportions than the other emission inventories during the spring season,
737 especially for PM₁₀. However, the proportion of emissions during autumn and winter are lower than in the other inventories.
738 The monthly profiles of NMVOC emissions are generally consistent, with higher emissions during summer due to the enhanced
739 biogenic emissions. However, the profile of CAQIEI is flatter than the previous inventories, and suggests a higher proportion
740 during springtime. In addition, the timings of peak values of NMVOC emissions are also different between CAQIEI and the



741 previous inventories, with CAQIEI showing peak values during May–July but the other inventories suggesting peaks during
742 June–August.

743 4.3.3 Emission changes during 2015–2018

744 The top-down estimated emission changes of different air pollutants during 2015–2018 were also compared with previous
745 emission inventories, the results of which are shown in Fig. 13. Before the comparison, we firstly analyze the trends of natural
746 sources in China to investigate their influences on the emission changes of different species. Note that we only consider the
747 soil, biogenic and biomass-burning emissions for the natural sources; the trends of dust emissions in China are not analyzed,
748 which may lead to uncertainty when comparing the emission changes of PM_{2.5} and PM₁₀. As shown in Fig. S7, the natural
749 sources of NO_x and NMVOC emissions changed little during 2013–2018, suggesting that the emission trends of these two
750 species would be mainly driven by anthropogenic sources. The other species had small decreasing trends from 2013 to 2018.
751 However, considering the small contributions of natural sources to their emissions, these small trends would not significantly
752 influence their emission trends. For the dust emissions, previous studies have indicated a declining trend in dust activity in
753 China from 2001 to 2020 (Wu et al., 2022; Wang et al., 2021), due to weakened surface wind and increased vegetation cover
754 and soil moisture. Thus, there would be declining trends in dust emissions in China, which should be noted when comparing
755 the emission changes of PM_{2.5} and PM₁₀.

756 As shown in Fig. 13, all the emission inventories agree that the NO_x, SO₂, CO, PM_{2.5} and PM₁₀ emissions in China were
757 reduced from 2015 to 2018, except for the increases of CO emissions estimated by TCR-2, which confirms the effectiveness
758 of the emission control policies implemented during the clean air action plans. Meanwhile, most emission inventories agree
759 that SO₂ is the species with the largest emission reductions, followed by PM_{2.5}, indicating better emission mitigation effects of
760 these two species. However, the emission reduction rates estimated by CAQIEI are generally lower than those estimated by
761 previous emission inventories, especially for NO_x, PM₁₀ and NMVOCs, which suggests that the mitigation effects of the air
762 quality control during 2015–2018 may be overestimated by previous inventories. The estimated emission reduction rate of
763 NO_x obtained from CAQIEI is about –2.7%, which is lower than the values of MEIC (–9.7%), ABaCAS (–23.0%), HTAPv3
764 (–13.0%) and CEDS (–9.0%). According to Fig. S8, the differences between CAQIEI and these inventories mainly occur in
765 the SE, SW, NW and Central regions, with the emission reduction rate estimated by CAQIEI being substantially lower than
766 those estimated by previous inventories. In particular, CAQIEI suggests increases of NO_x emissions over the Central region,
767 which was not captured by previous inventories. Better agreement is achieved over the NCP and NE regions, with the emission
768 reduction rate estimated by CAQIEI being closer to those of MEIC, HTAPv3 and CEDS, suggesting lower uncertainty in the
769 estimated NO_x emission reduction rate over these two regions. The NO_x emission reduction rates estimated by EDGARv6
770 (–3.3%) and TCR-2 (–1.7%) are closer to our results on the national scale, but they underestimate the NO_x emission reduction
771 rate over the NCP and NE regions.

772 Similarly, the emission reduction rate of PM₁₀ obtained from CAQIEI (–10.8%) is much lower than those estimated by
773 MEIC (–27.9%), ABaCAS (–33.0%) and HTAPv3 (–27.8%) on the national scale (Fig. 13). A lower PM₁₀ emission reduction
774 rate of CAQIEI than these inventories also exists in the different regions of China, except SW (Fig. S8). In particular, different
775 from previous emission inventories, CAQIEI suggests that PM₁₀ emissions may have actually increased over the Central region.
776 Considering that dust emissions may have decreased from 2015 to 2018 owing to weakened dust events (Wang et al., 2021),
777 the increase in PM₁₀ emissions over the Central region may reflect the increases in anthropogenic sources. Meanwhile, we also
778 found that CAQIEI estimated the emission reduction rate of PM₁₀ to be smaller than that of PM_{2.5}. This is different from
779 previous emission inventories, which show similar emission reduction rates for PM_{2.5} and PM₁₀. Considering that PM₁₀
780 emissions include PM_{2.5} and PMC emissions, the lower emission reduction rate of PM₁₀ than PM_{2.5} in CAQIEI suggests that
781 PMC emissions may have decreased slower than PM_{2.5} emissions from 2015 to 2018, which was not captured by previous
782 inventories.



783 In terms of NMVOCs, most previous inventories, including MEIC, EDGARv6 and CEDS, suggest a weak decrease in
784 China, with the estimated rates of change in emissions ranging from -0.8% to -4.6% . The emission reduction rate estimated
785 by ABaCAS is larger, reaching up to -14.2% . In contrast, CAQIEI indicates an opposite emission change to these inventories,
786 with estimated NMVOC emissions increasing by 26.6% from 2015 to 2018. HATPv3 also suggests an increase in NMVOC
787 emissions, but with a much lower rate of increase (2.7%). Similar results could also be found on the regional scale (Fig. S8),
788 especially over the NCP, NE and Central regions, where NMVOC emissions could have increased by 38.0% , 38.3% and 60.0% ,
789 respectively, according to the estimates of CAQIEI. However, none of the previous emission inventories captured this
790 increasing trend over these regions. Considering that biogenic NMVOC emissions changed little from 2015 to 2018 according
791 to the estimates of the CAMS inventory, the increases of NMVOC emissions possibly arise from the increased anthropogenic
792 sources. This is consistent with the estimate of Li et al. (2019c), who found persistent growth of anthropogenic NMVOC
793 emissions in China from 1900 to 2017. However, the drivers of the increased NMVOC emissions still need to be investigated,
794 considering the uncertainty in the estimated trends of biogenic NMVOC emissions. Different from the CAMS inventory, Li et
795 al. (2020a) found an increasing trend in biogenic emissions in China from 2008 to 2018, especially over northern China, which
796 can partly explain the increased NMVOC emissions in China. Therefore, more analysis is needed to better understand the
797 potential drivers of the increased NMVOC emissions in China.

798 The differences in the estimated emission reduction rates between CAQIEI and previous inventories are relatively smaller
799 for SO_2 and $\text{PM}_{2.5}$ emissions, suggesting lower uncertainty in the estimated emission reduction rates for these two species. The
800 emission reduction rate of SO_2 estimated by CAQIEI is close to that estimated by MEIC and CEDS, ranging from -34.7% to
801 -44.3% . ABaCAS and HTAPv3 estimate a larger emission reduction rate of about -58.5% and -53.7% , respectively.
802 EDGARv6 and TCR-2 may greatly underestimate the reduction rate of SO_2 , with estimates of only about -7.0% and -9.1% ,
803 respectively. This may be because EDGARv6 underestimates the FGD (flue-gas desulfurization devices) penetration or SO_2
804 removal efficiencies of FGD in China. On the regional scale (Fig. S8), the top-down estimated SO_2 emission reduction rate
805 agrees reasonably with that of MEIC over the NCP, NE and SE regions, but these inventories estimate different SO_2 emission
806 reduction rates over the SW, NW, and Central regions. The reduction rates estimated by MEIC over the SW and Central
807 regions is higher than those given by CAQIEI, but lower over the NW region. The other emission inventories also give different
808 emission reduction rates. For example, CEDS shows similar results to our estimate over the SW and Central regions, while the
809 rate given by HTAPv3 is closer to MEIC. This suggests there are high levels of uncertainty in the estimated SO_2 emission
810 reduction rates over these three regions. In terms of $\text{PM}_{2.5}$, CAQIEI's estimated emission reduction rate agrees well with those
811 of MEIC and HTAPv3 on the national scale, suggesting that the emission reduction rate of $\text{PM}_{2.5}$ in China was about $24\text{--}27\%$
812 from 2015 to 2018. EDGARv6 may underestimate the reduction rate of $\text{PM}_{2.5}$, at about 9% . On the regional scale, our results
813 show good consistency with MEIC and HTAPv3 over the NCP, NE, SE and SW regions, but they have large differences over
814 the NW and SW regions, indicating higher uncertainty in the estimated reduction rate over western China.

815 Different from the other species, the CO emission reduction rate estimated by CAQIEI (-21.3%) is higher than in most
816 of the previous inventories, including MEIC (-13.0%), ABaCAS (-11.6%), EDGARv6 (-4.7%), and CEDS (-11.7%),
817 suggesting that the mitigation effects on CO emissions may be underestimated by these inventories. HTAPv3 agrees with our
818 results, with an estimated emission reduction rate of about -22.0% . On the regional scale (Fig. S8), our result is consistent
819 with MEIC over the NCP and SE regions, with estimated emission reduction rates for CO of around 24% and 15% , respectively,
820 while in other regions the emission reduction rate estimated by CAQIEI is higher than that estimated by MEIC. The larger
821 emission reduction rate for CO in our results is supported by HTAPv3 over the NE, SW, NW and Central regions, as well as
822 by CEDS over the SW, NW and Central regions. This suggests that the emission reduction rates for CO may be underestimated
823 by MEIC over these regions. TCR-2 shows opposite changes in CO emissions compared with the other inventories insofar as
824 it suggests increases of CO emissions over different regions of China. Since the emissions in TCR-2 are constrained by satellite
825 observations, the differences between our results and those of TCR-2 highlight that the observations used to constrain the



826 emissions may have a large influence on the estimated emission changes. In this case, the assimilation of surface observations
827 (our study) is shown to be superior to the assimilation of satellite observations (TCR-2), as our results are more consistent with
828 other bottom-up inventories.

829 **5 Discussion and conclusion**

830 A long-term, top-down emissions inventory of major air pollutants in China was developed and validated in this study by
831 assimilating surface observations from CNEMC using the modified EnKF method and NAQPMS. It includes gridded emission
832 maps of NO_x, SO₂, CO, primary PM_{2.5}, primary PM₁₀, and NMVOCs in China from 2013 to 2020, on a monthly basis, with a
833 horizontal resolution of 15 km × 15 km. This new top-down emissions inventory, named CAQIEI, provides new insights into
834 the air pollutant emissions and their changes in China during the country's two clean air action periods, which has not been
835 reported by previous inventories. The estimated total emissions for the year 2015 in China are 25.2 Tg of NO_x, 17.8 Tg of SO₂,
836 465.4 Tg of CO, 15.0 Tg of PM_{2.5}, 40.1 Tg of PM₁₀ and 46.0 Tg of NMVOCs. Comparisons of CAQIEI with previous
837 inventories, including MEIC, ABaCAS, HTAPv3, EDGARv6, CEDS and TCR-2, showed reasonable agreement for the
838 estimation of NO_x, SO₂ and NMVOC emissions in China, which confirms our inversion results and suggests lower uncertainty
839 in the estimated total emissions in China for these species. The PM_{2.5} emissions obtained from CAQIEI (13.2 Tg) are slightly
840 higher than in the previous emission inventories (8.3–11.1 Tg), suggesting possible underestimations of the anthropogenic,
841 biomass-burning or fine-dust emissions in current estimations. The CO emissions estimated by CAQIEI (426.8 Tg) are
842 substantially higher than in previous inventories (120.7–237.7 Tg), indicating that CO emissions may be greatly
843 underestimated currently. Although previous model simulation and inversion studies generally support the underestimation of
844 CO emissions in China, the reasons for such a large underestimation are still not clear, but might be attributable to both the
845 underestimation of CO sources, e.g., anthropogenic, biomass-burning and chemical-production sources, and/or the
846 overestimation of CO sinks. In addition, comparisons with previous inversion studies suggest there are larger differences in
847 the top-down estimated CO emissions based on surface and satellite observations. Our inversion results are consistent with
848 previous inversions based on surface observations, but are much higher than those based on satellite observations, suggesting
849 large uncertainty in inversion-estimated CO emissions in China. Therefore, more research is needed to better understand the
850 reasons behind the negative biases in CO simulation, and to explain the differences between our results and those of previous
851 inventories. Similar to situation with CO emissions, the PM₁₀ emissions estimated by CAQIEI (37.7 Tg) are also substantially
852 higher than in previous inventories (11.1–15.9 Tg). However, this will be mainly associated with the emissions of coarse dust,
853 which were not included in previous inventories. The estimation of dust emissions in China is subject to high levels of
854 uncertainty, with the estimated dust fluxes based on different dust emission schemes differing by several orders of magnitude
855 (Zeng et al., 2020). Therefore, our inversion results could provide a reference for the magnitude of coarse-dust emissions in
856 China, which could then help to reduce the large uncertainty in estimations of dust emissions in China.

857 Several potential important deficiencies in current emission estimations were also revealed by CAQIEI on the regional
858 scale. For example, there are significant negative biases in the estimated air pollutant emissions over the NW and Central
859 regions, suggesting that the air pollutant emissions in western China may be greatly underestimated by current emission
860 inventories. As a result, significant air pollutant issues may be neglected over these two regions, which may have led to serious
861 adverse impacts in terms of human health and ecosystems. Meanwhile, NMVOC emissions are shown to be substantially
862 underestimated over northern China but overestimated in southern China. China is now facing increasingly severe O₃ pollution
863 and has an urgent need for a coordinated control of O₃ and PM_{2.5}. Our results shed new light on the nature of NMVOC
864 emissions in China, which is important for a proper understanding of O₃ pollution and the development of effective control
865 strategies nationally. Consistent negative biases were also identified in the NE region for the emissions of all species. The NE
866 region is a typical area for open-area biomass burning, with significant emissions from straw combustion (Wu et al., 2020b).



867 The underestimation of emissions there may reflect the underestimation of biomass-burning emissions. This is consistent with
868 recent estimations of biomass-burning emissions by Xu et al. (2023) and Wu et al. (2020b), who showed higher biomass-
869 burning emissions in China than previous estimations, including those of GFEDv4.1s
870 (<https://www.globalfiredata.org/data.html>), FINNv1.5 (<https://www.acom.ucar.edu/Data/fire/>), and GFASv1.2
871 (<https://www.ecmwf.int/en/forecasts/dataset/global-fire-assimilation-system>).

872 Based on CAQIEI, we further quantified the emission changes of different air pollutants in China during the two clean
873 air action plans. The results confirmed the effectiveness of these campaigns on the mitigation of air pollutant emissions in
874 China, with estimated emission reductions of 15.1% for NO_x, 54.5% for SO₂, 35.7% for CO, 44.4% for PM_{2.5}, and 33.6% for
875 PM₁₀ from 2015 to 2020. In contrast, NMVOC emissions increased by 21.0% from 2015 to 2020. Comparisons of the estimated
876 emission reduction rates during the two clean air action plans suggested that emission reductions were larger during the 2018–
877 2020 action plan than during the 2013–2017 action plan. The estimated rates of change in emissions were 5.9% for NO_x, –23.8%
878 for SO₂, –9.8% for CO, –14.5% for PM_{2.5}, –7.2% for PM₁₀, and 27.6% for NMVOCs during the 2013–2017 action plan, which
879 were smaller than the –12.1% for NO_x, –23.5% for SO₂, –18.3% for CO, –26.6% for PM_{2.5}, –25.5% for PM₁₀, and –4.5% for
880 NMVOCs during the 2018–2020 action plan. On the one hand, this is due to the fact that more sectors were controlled during
881 the 2018–2020 action plan. Besides the industrial and power sectors, which were the main points of control in the 2013–2017
882 action plan, the residential sector, transportation sector, and non-point sources like blowing-dust emissions, were also
883 strengthened in the 2018–2020 action plan. Consequently, the emission reduction rates of CO, PM_{2.5} and PM₁₀ during the
884 2018–2020 action plan were higher than those during the 2013–2017 action plan. However, the reduction of SO₂ emissions
885 was similar during the two action plan periods. This is because most SO₂ emissions stem from the industrial sector and power
886 plants, which together contribute about 77% of all emissions (Zheng et al., 2018). Thus, the additional control of other sectors
887 in the 2018–2020 action plan may not have significantly impacted the mitigation of SO₂ emissions. On the other hand, strict
888 emission controls were implemented or strengthened in more areas of China during the 2018–2020 action plans. For example,
889 the inversion results indicated that there were obvious increases of SO₂, NO_x, PM_{2.5}, PM₁₀ and NMVOC emissions during the
890 2013–2017 action plan over the Central region, especially in the Fengwei Plain area, where the emission controls were
891 relatively weak during the 2013–2017 action plan. However, all species showed obvious emission reductions over the Fengwei
892 Plain area, and almost the whole of China, during the 2018–2020 action plan.

893 The estimated rates of change in emissions during 2015–2018 were also compared with those estimated by previous
894 emission inventories. Although both CAQIEI and previous inventories showed declines of air pollutant emissions in China,
895 the emission reduction rates estimated by CAQIEI were generally smaller than those estimated by previous inventories,
896 especially for NO_x, PM₁₀ and NMVOCs, suggesting that the mitigation effects of the air pollution control measures may be
897 overestimated currently. In particular, China's NMVOC emissions were shown to have increased by 26.6% from 2015 to 2018,
898 especially over NCP (38.0%), NE (38.3%) and Central (60.0%), which was not captured by all previous inventories. The
899 potential overestimation of the NO_x emission reduction rate was mainly a feature of the SE, SW, NW and Central regions;
900 however, over the NCP and NE regions, our results agreed well with those of MEIC, HTAPv3 and CEDS, suggesting smaller
901 uncertainty in the estimated reduction of NO_x emissions over these two regions. The potential overestimation of the PM₁₀
902 emission reduction rate was a feature in most regions of China, possibly related to the smaller reduction rate of the country's
903 PM₁₀ emissions. CO was found to be an exception insofar as the emission reduction rate estimated by CAQIEI was larger than
904 that of most previous emission inventories, suggesting that the mitigation effects of CO emission control measures may be
905 underestimated, except in the NCP region. The estimated emission reduction rates of SO₂ and PM_{2.5} were relatively closer to
906 those of previous inventories, suggesting relatively lower uncertainty in the estimated pace of emission reduction for these two
907 species.

908 Overall, the inversion inventory developed in this study sheds new light on the complex variations of air pollutant
909 emissions in China during its two recent clean air action periods, which could significantly improve our understanding of air



910 pollutant emissions and related changes in air quality in China. For example, the increases of O₃ and nitrate concentrations
911 may be associated with the undesirable emission reduction effects of the 2013–2017 action plans. The possible overestimation
912 of the NO_x emission reduction rate by previous inventories may also help explain the weak responses of nitrogen deposition
913 fluxes to the clean air action plans. Meanwhile, this top-down emissions inventory can be used to supply the input data for
914 CTMs, which is expected to improve the performance of model simulations and air quality forecasts. However, there are some
915 limitations to our inventory that potential users should be aware of. Firstly, the changes in the number of observation sites may
916 have induced spurious emission trends during 2013–2014, especially over western China, although the influence of the number
917 of observation sites is smaller over the NCP and SE regions because of their higher density of observation sites. In addition,
918 although the number of observation sites has become stable since 2015, the limited number of observation sites makes it
919 difficult to fully constrain China’s air pollutant emissions, especially with respect to natural sources in remote areas. For
920 example, the coarse-dust emissions over western China are expected to be underestimated by CAQIEI because of the limited
921 availability of observation sites. Therefore, adding observations there will help improve the accuracy of the inversion estimates.
922 Secondly, natural and anthropogenic emissions are not differentiated in our inversion method, leading to higher emissions of
923 PM₁₀ and NMVOCs than in other emission inventories. Consequently, the estimated changes in emissions of different air
924 pollutants are also influenced by natural emissions, which should be considered in the comparisons of our inversion results
925 with those of previous emission inventories. Assimilation of isotope data, speciated PM_{2.5} and NMVOC observations may help
926 address this problem in future. Thirdly, the errors in the meteorological simulation and the CTMs were not considered in the
927 emission inversions, leading to uncertainty in our estimated emissions. However, it is difficult to consider the meteorological
928 and model errors in the assimilation process. A multi-model inversion framework, for example that of Miyazaki et al. (2020a),
929 may help alleviate the influences of model errors on emission inversions in future. Meanwhile, because of the many uses that
930 require a rapid update of emissions, it may be time to organize an intercomparison study focused on the emission inversions.

931 **6 data availability**

932 The CAQIEI inventory can be freely download at <https://doi.org/10.57760/sciencedb.13151> (Kong et al., 2023), which
933 includes monthly grid maps of the air pollutant emissions from 2013 to 2020. The contained species include NO_x, SO₂, CO,
934 primary PM_{2.5}, primary PM₁₀ and NMVOC. The horizontal resolution is 15km. There are totally 8 Network Common Data
935 Form files (NetCDF), which were named by the date and contains the monthly emissions of different air pollutants in China
936 in each year. The description of the content of each NetCDF file and some important notes when using this dataset are also
937 available in README.txt on the website.

938
939
940
941
942
943
944
945
946
947
948
949
950



951 **Tables**

952 **Table 1. Corresponding relationships between the chemical observations and adjusted emissions**

Species	Description	Observations used for inversions of this species
BC	Black carbon	PM _{2.5}
OC	Organic carbon	PM _{2.5}
PMF	Fine-mode unspiciated aerosol	PM _{2.5}
PMC	Coarse-mode unspiciated aerosol	PM ₁₀ – PM _{2.5}
NO _x	Nitrogen oxide	NO ₂
SO ₂	Sulfur dioxide	SO ₂
CO	Carbon monoxide	CO
NMVOCs	Non-methane volatile organic compounds	MDA8h O ₃

953
954
955
956
957
958
959
960
961
962
963
964
965
966
967
968
969
970
971
972
973
974
975
976
977
978
979
980
981



982 **Table 2. Evaluation statistics of the *a posteriori* (*a priori*) model simulation for different species**

	PM _{2.5} (µg/m ³)				PM ₁₀ (µg/m ³)			
	R	MBE	NMB (%)	RMSE	R	MBE	NMB (%)	RMSE
Hourly	0.77 (0.53)	2.1 (13.3)	4.5 (28.6)	32.4 (55.6)	0.72 (0.44)	-3.7 (-11.5)	-4.6 (-14.3)	53.1 (74.4)
Daily	0.89 (0.61)	2.1 (13.3)	4.4 (28.4)	20.0 (46.3)	0.88 (0.51)	-3.7 (-11.2)	-4.6 (-14.1)	31.6 (62.2)
Monthly	0.94 (0.68)	2.1 (13.3)	4.5 (28.3)	11.7 (32.5)	0.90 (0.56)	-3.6 (-11.3)	-4.5 (-14.1)	21.2 (44.1)
Yearly	0.94 (0.62)	2.2 (11.9)	4.4 (24.3)	9.1 (27.7)	0.89 (0.52)	-3.8 (-13.4)	-4.6 (-16.1)	18.5 (38.7)
	SO ₂ (µg/m ³)				NO ₂ (µg/m ³)			
	R	MBE	NMB (%)	RMSE	R	MBE	NMB (%)	RMSE
Hourly	0.64 (0.16)	-1.8 (19.0)	-9.1 (93.8)	24.9 (58.7)	0.67 (0.45)	-1.2 (-0.9)	-3.9 (-2.7)	19.9 (25.5)
Daily	0.80 (0.20)	-1.8 (19.0)	-9.2 (94.5)	16.0 (51.4)	0.80 (0.51)	-1.2 (-0.8)	-3.7 (-2.6)	12.8 (20.1)
Monthly	0.85 (0.20)	-1.9 (18.9)	-9.3 (93.1)	12.4 (45.8)	0.84 (0.57)	-1.2 (-0.8)	-3.8 (-2.6)	9.4 (15.6)
Yearly	0.83 (0.18)	-2.4 (17.0)	-10.8 (75.9)	11.6 (42.4)	0.82 (0.63)	-1.3 (-1.6)	-3.9 (-5.0)	8.1 (13.0)
	CO (mg/m ³)				O ₃ (µg/m ³)			
	R	MBE	NMB (%)	RMSE	R	MBE	NMB (%)	RMSE
Hourly	0.69 (0.38)	-0.1 (-0.4)	-8.8 (-45.6)	0.6 (0.8)	0.71 (0.51)	5.6 (-8.4)	9.5 (-14.0)	34.9 (41.6)
Daily	0.81 (0.42)	-0.1 (-0.4)	-8.6 (-45.5)	0.4 (0.7)	0.71 (0.40)	5.7 (-8.4)	9.5 (-14.1)	26.1 (33.8)
Monthly	0.83 (0.42)	-0.1 (-0.4)	-8.7 (-45.7)	0.3 (0.7)	0.76 (0.47)	5.6 (-8.4)	9.4 (-14.1)	19.6 (26.0)
Yearly	0.82 (0.27)	-0.1 (-0.5)	-9.0 (-47.6)	0.3 (0.7)	0.53 (0.11)	5.1 (-7.8)	8.7 (-13.4)	14.2 (20.5)

983
 984
 985
 986
 987
 988
 989
 990
 991
 992
 993
 994
 995
 996
 997
 998
 999
 1000
 1001



1002 **Table 3. Inversion-estimated emissions (Tg/yr) of different species in China as well as the six regions**

	China	NCP	SE	NE	SW	NW	Central
NO _x	25.2	5.1	7.1	4.5	4.2	1.2	3.2
SO ₂	17.8	3.5	3.3	4.0	2.6	0.8	3.6
CO	465.4	82.2	106.7	78.7	82.8	32.6	82.3
PM _{2.5}	14.9	2.7	3.3	3.1	2.9	1.2	1.9
PM ₁₀	40.1	8.7	7.5	8.2	5.5	4.1	6.2
NMVOC	46.0	9.0	13.7	8.5	7.8	2.7	4.2

1003
 1004
 1005
 1006
 1007
 1008

1009 **Table 4. The calculated annual trends of PM_{2.5} and PM₁₀ emissions in China based on CAQIEI**

	PM _{2.5} (Tg/year)			PM ₁₀ (Tg/year)		
	2015–2020	2015–2017	2018–2020	2015–2020	2015–2017	2018–2020
China	-1.4*	-1.1	-1.5	-2.6*	-1.4	-4.6
NCP	-0.32*	-0.30	-0.32	-0.64*	-0.88	-0.99
SE	-0.32*	-0.21	-0.44	-0.52*	-0.48	-0.84
NE	-0.24*	-0.25	-0.11	-0.52*	-0.22	-0.73
SW	-0.21*	-0.26	-0.20	-0.40*	-0.26	-0.56
NW	-0.09	-0.08	-0.12	-0.20*	-0.32	-0.32
Central	-0.15	0.01	-0.32	-0.27	-0.32	-1.14

* Trend is significant at the 0.05 significance level

1010
 1011
 1012
 1013
 1014
 1015
 1016
 1017
 1018
 1019
 1020
 1021
 1022
 1023
 1024
 1025
 1026
 1027
 1028



1029 **Table 5. The calculated annual trends of the four gaseous emissions in China based on CAQIEI**

	SO ₂ (Tg/year)			CO (Tg/year)		
	2015–2020	2015–2017	2018–2020	2015–2020	2015–2017	2018–2020
China	–2.1*	–2.1	–1.3	–36.0*	–22.8	–33.5
NCP	–0.57*	–0.69	–0.21	–8.4*	–4.30	–7.23
SE	–0.34*	–0.39	–0.20	–6.1*	–3.54	–8.37
NE	–0.44*	–0.44	–0.21	–6.2*	–1.74	–3.91
SW	–0.22*	–0.27	–0.17	–3.8*	–2.36	–4.54
NW	–0.08*	–0.08	–0.08	–3.0*	–0.73	–2.95
Central	–0.46*	–0.25	–0.40	–8.7*	–10.14	–6.55
	NO _x (Tg/year)			NMVOC (Tg/year)		
	2015–2020	2015–2017	2018–2020	2015–2020	2015–2017	2018–2020
China	–0.67	0.74	–1.6	1.9	6.3	–1.3
NCP	–0.32	0.05	–0.40	0.66	1.37	–0.42
SE	–0.22	0.18	–0.49	0.50	1.73	–0.24
NE	–0.17	0.03	–0.19	0.03	0.79	–0.49
SW	–0.06	0.10	–0.26	0.23*	0.43	0.03
NW	–0.03	0.11	–0.06	0.10	0.69	–0.27
Central	0.04	0.28	–0.16	0.55*	1.33	0.09

* Trend is significant at the 0.05 significance level

1030
 1031
 1032
 1033
 1034
 1035
 1036
 1037
 1038
 1039
 1040
 1041
 1042
 1043
 1044
 1045
 1046
 1047
 1048
 1049
 1050
 1051
 1052
 1053



1054 **Table 6 The top-down estimated CO emissions in China from previous inventories**

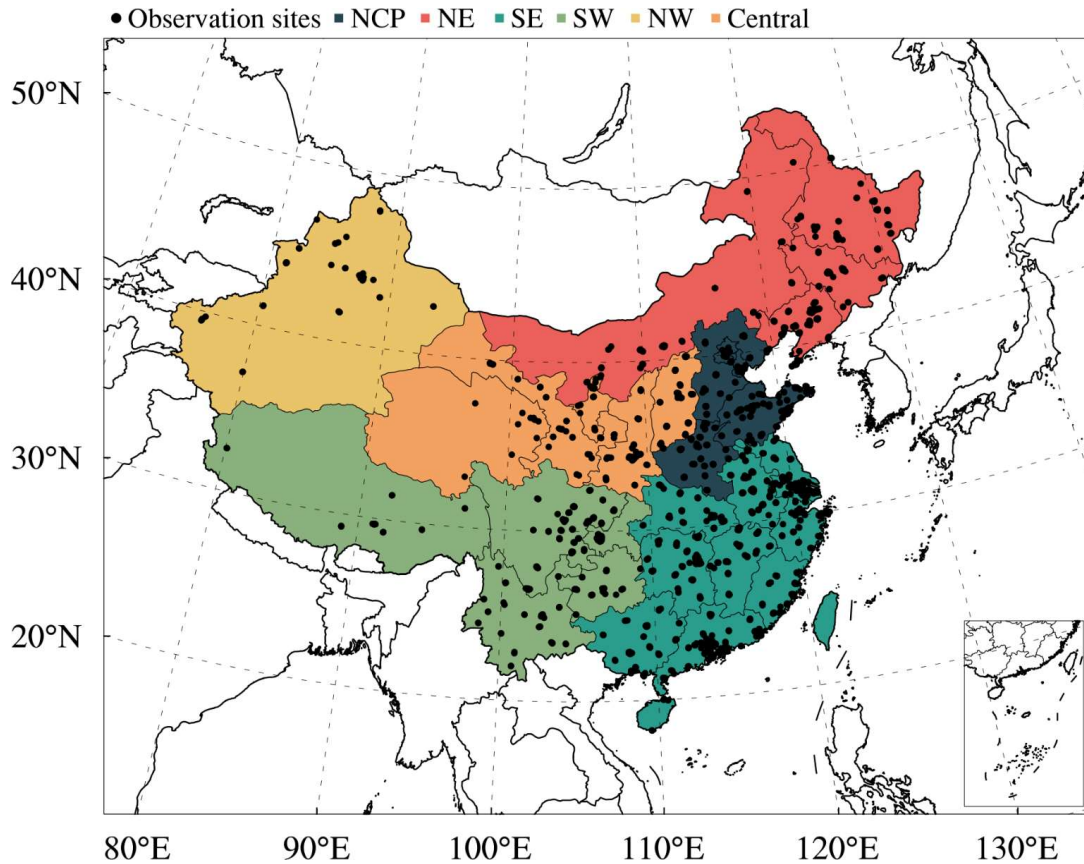
Reference	Region	Period	Method	Assimilated observation	<i>A priori</i> CO emission (kt/day)	<i>A posteriori</i> CO emission (kt/day)
Feng et al. (2020)	China	December 2013			586.4	1678.0
	Mainland	December 2017	EnKF with	Surface	499.3	1388.1
	NCP	December 2013	CMAQ model	observation	143.9	394.3
		December 2017			120.5	340.7
Muller et al. (2018)	China	2013	4DVar with IMAGES model	IASI CO observation with different constraints on OH levels	454.8	367.1–553.4
Gaubert et al. (2020)	Central China	May 2016	DART/CAM-CHEM	MOPITT CO observation	193.6	220.3
	North China				93.5	163.6
Jiang et al. (2017)	East China	2013	4DVar with GEOS-Chem	MOPITT CO observation	564.5	439.5–484.4
		2014				430.4–481.1
		2015				397.5–439.7
Zheng et al. (2019)	China	2010–2017 average	Bayesian inversion	MOPITT CO, OMI HCHO, and GOSAT CH ₄ observation	-	444.4

1055
1056
1057
1058
1059
1060
1061
1062
1063
1064
1065
1066
1067
1068
1069
1070



1071 **Figures**

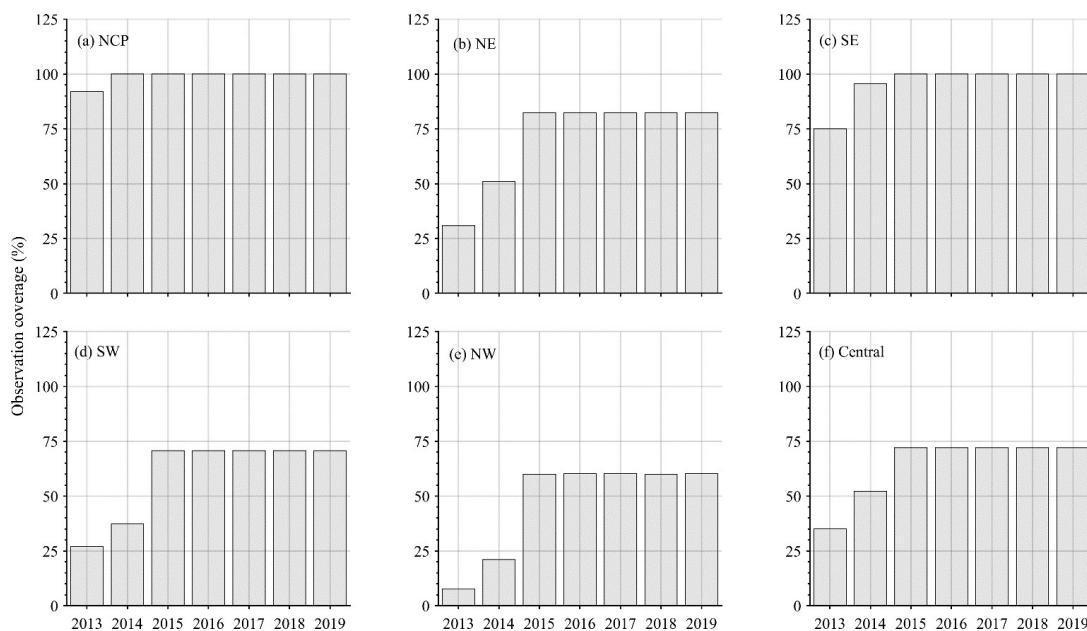
1072



1073

1074 **Figure 1: Modeling domain of the ensemble simulation overlaid with the distributions of observation sites from CNEMC. Different**
1075 **colors denote the different regions in mainland China—namely, the North China Plain (NCP), Northeast China (NE), Southwest**
1076 **China (SW), Southeast China (SE), Northwest China (NW) and Central China (Central).**

1077



1078

1079 **Figure 2: Time series of the observational coverage from 2013 to 2020 over different regions of China.**

1080

1081

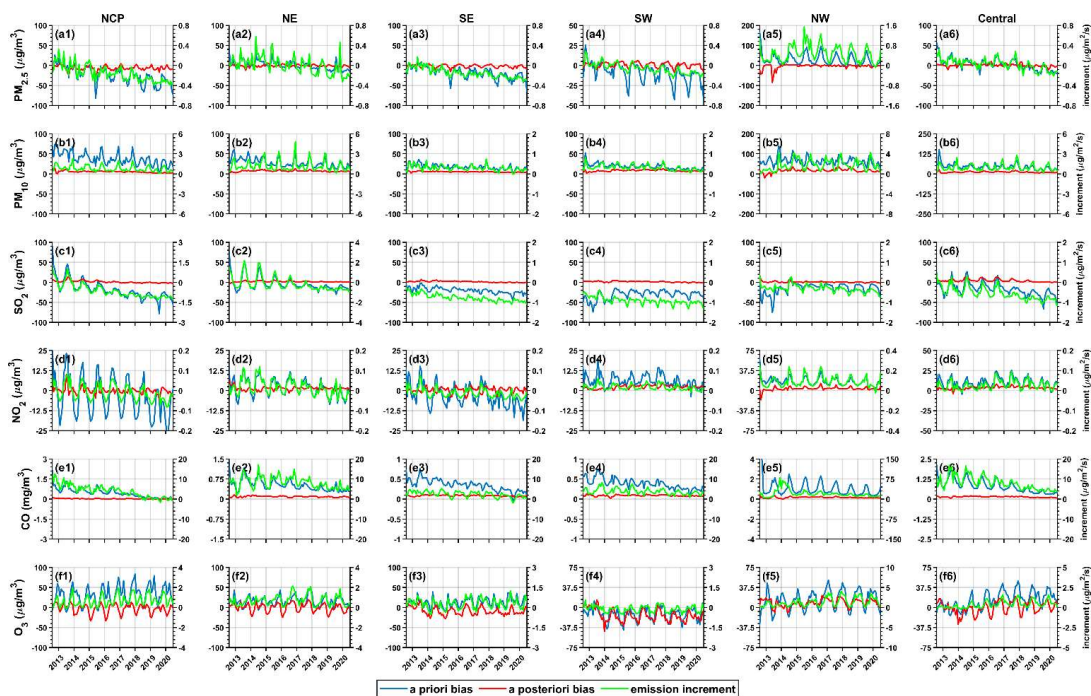
1082

1083

1084

1085

1086



1087

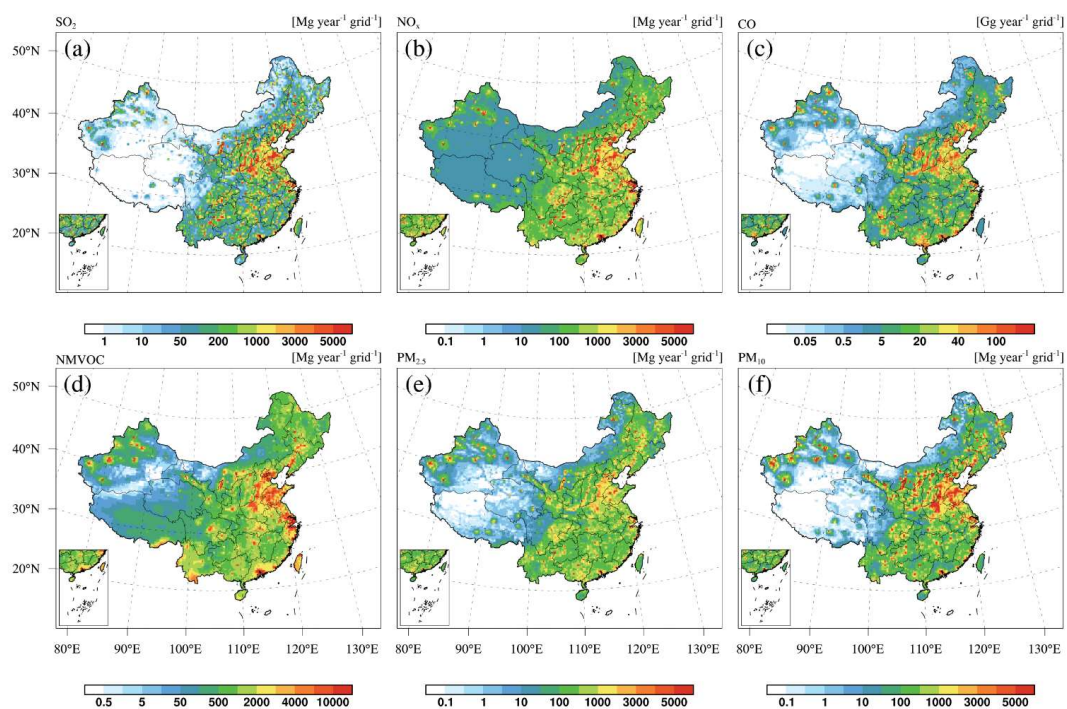
1088

1089

Figure 3: Time series of the *a priori* bias (blue lines), the *a posteriori* bias (red lines), and the emission increment (green lines) from 2013 to 2020 for different species over the six regions of China.

1090

1091



1092

1093

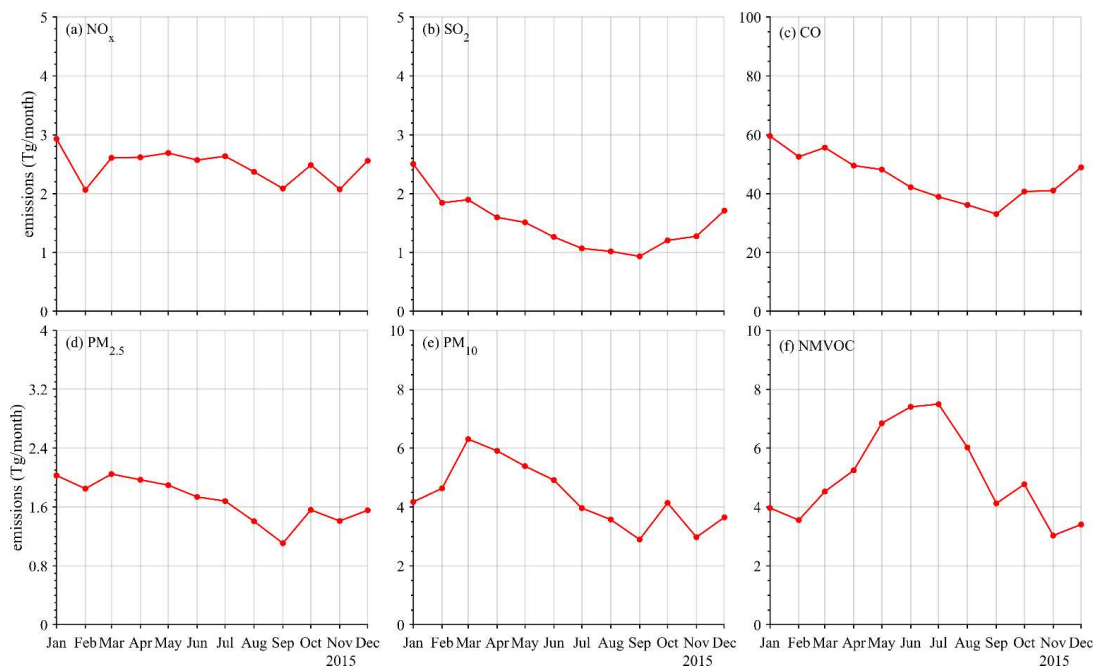
1094

Figure 4: Spatial distributions of the emissions of (a) SO₂, (b) NO_x, (c) CO, (d) NMVOCs, (e) PM_{2.5}, and (f) PM₁₀ in 2015 obtained from CAQIEL.

1095

1096

1097



1098

1099

1100

Figure 5: Monthly series of emissions of (a) NO_x, (b) SO₂, (c) CO, (d) PM_{2.5}, (e) PM₁₀, and (f) NMVOCs in 2015 obtained from CAQIEI.

1101

1102

1103

1104

1105

1106

1107

1108

1109

1110

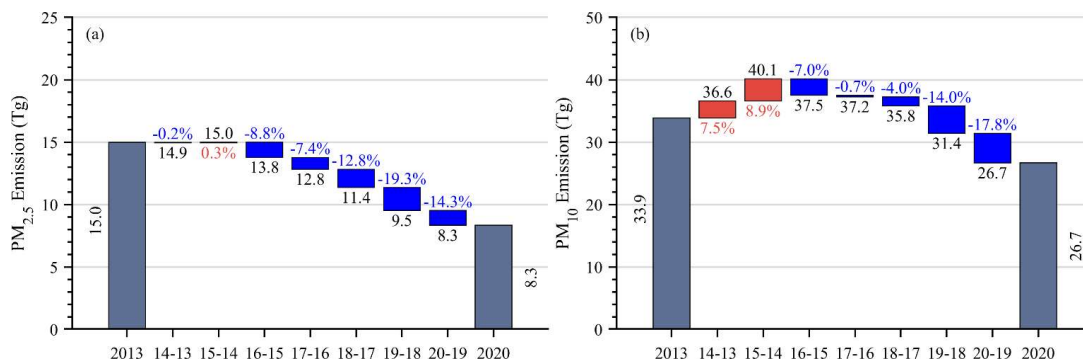
1111

1112

1113

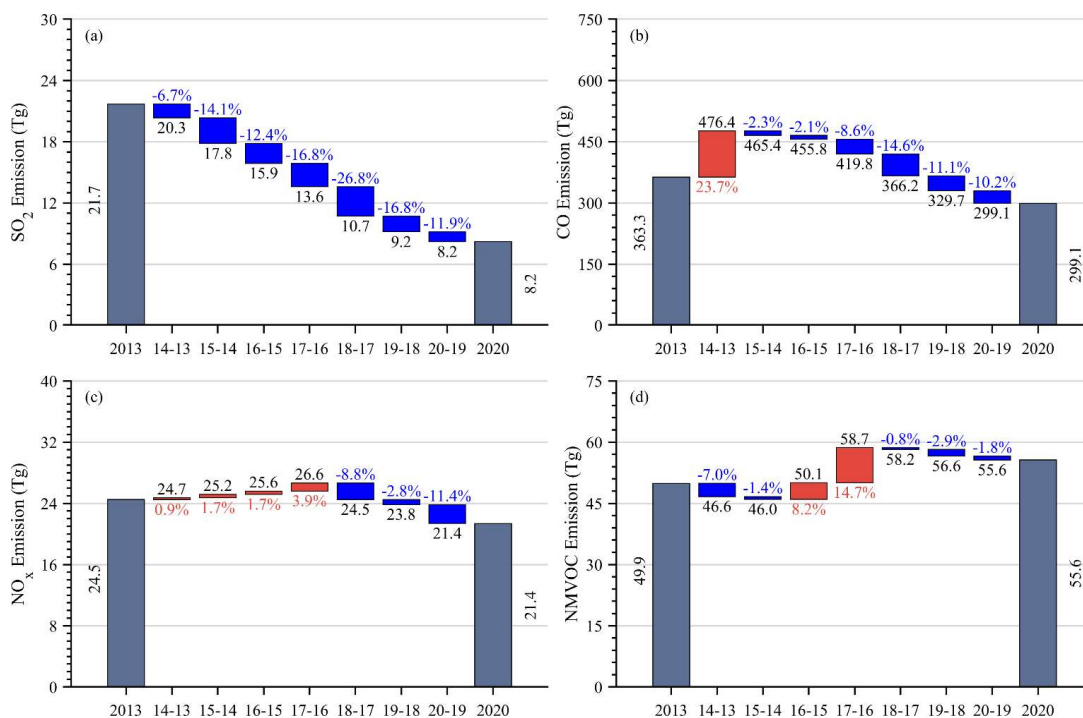
1114

1115



1116

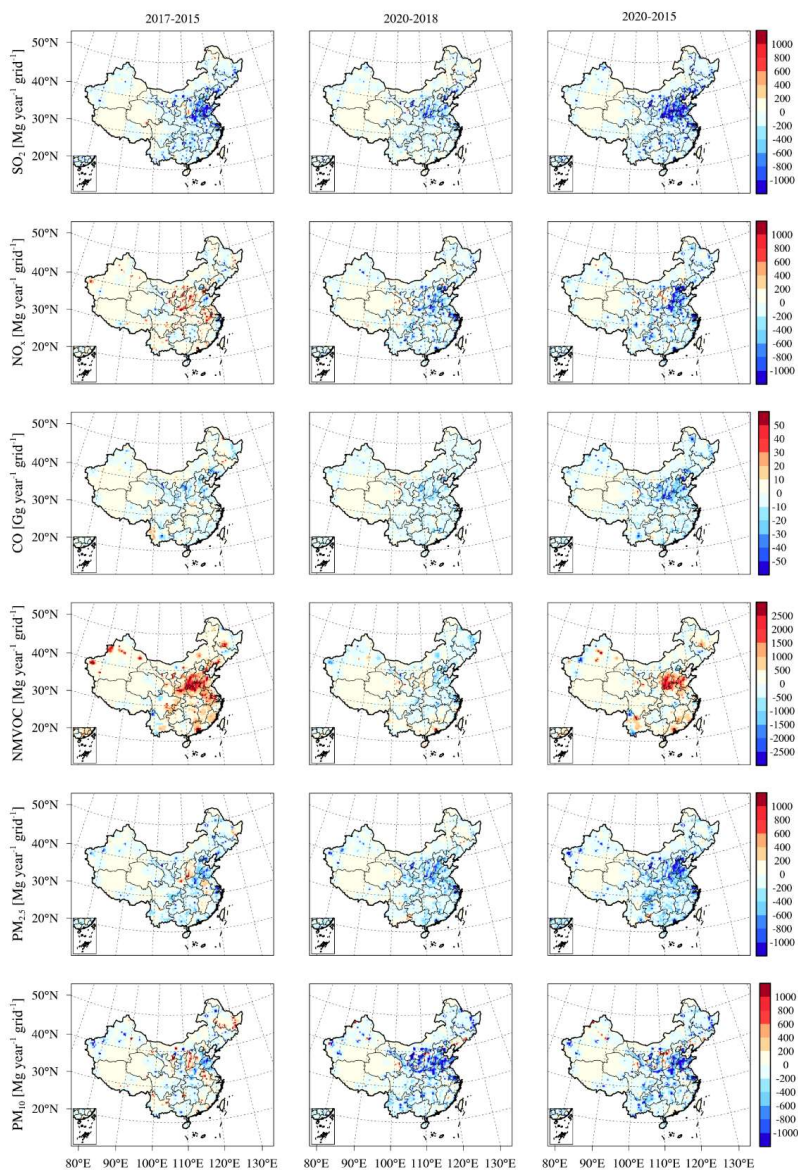
1117 **Figure 6: Emission changes in (a) PM_{2.5} and (b) PM₁₀ obtained from CAQIEI from 2013 to 2020.**



1118

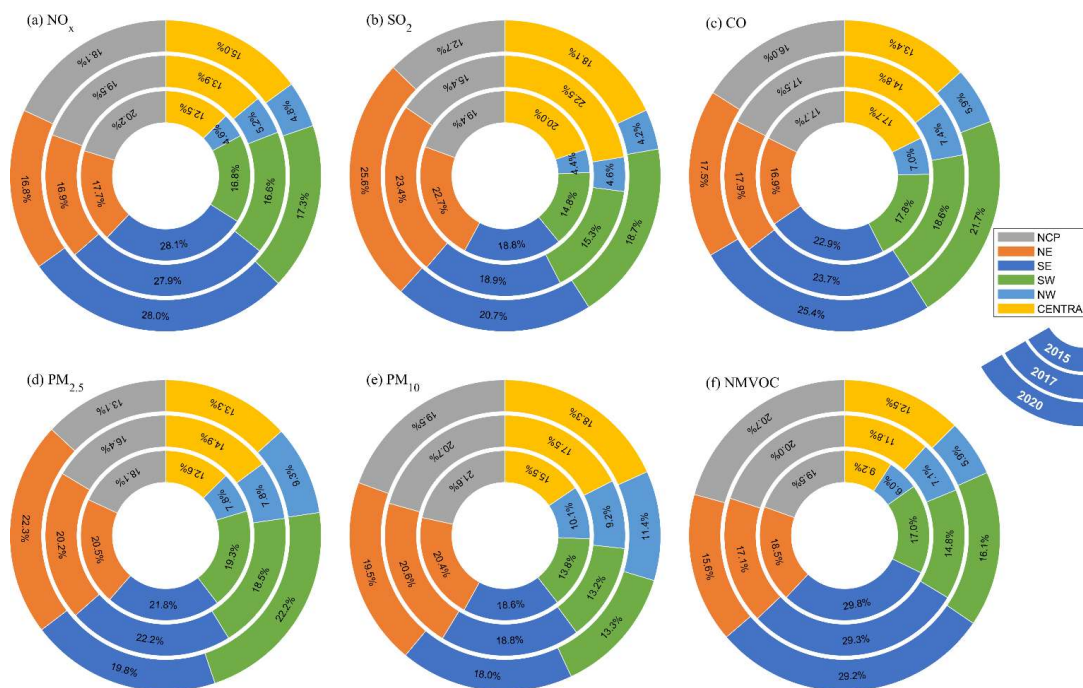
1119 **Figure 7: Emission changes in (a) SO₂, (b) CO, (c) NO_x, and (d) NMVOCs obtained from CAQIEI from 2013 to 2020.**

1120



1121

1122 **Figure 8:** Spatial distributions of the emission changes of different species during 2015–2017 (left panels), 2018–2020 (middle panels),
1123 and 2015–2020 (right panels) obtained from CAQIEI from 2013 to 2020.

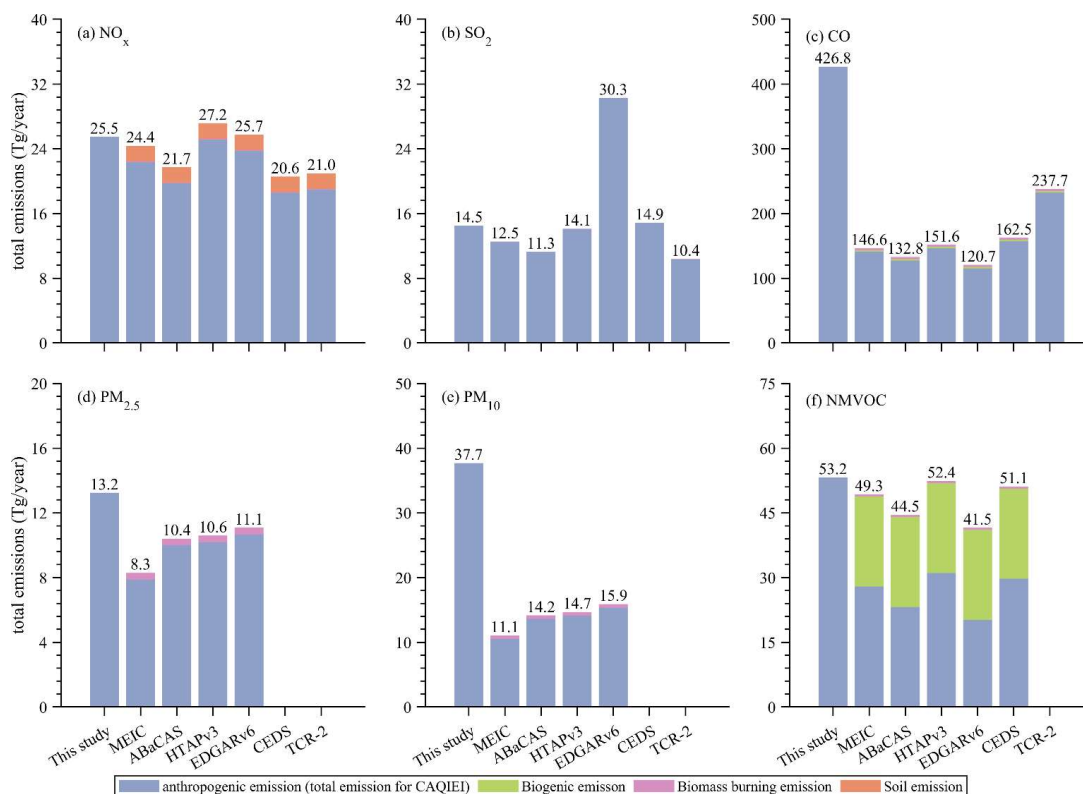


1124

1125 **Figure 9: Emission distributions of (a) NO_x, (b) SO₂, (c) CO, (d) PM_{2.5}, (e) PM₁₀, and (f) NMVOCs among different regions in China**
 1126 **obtained from CAQIEI in 2015, 2017 and 2020.**

1127

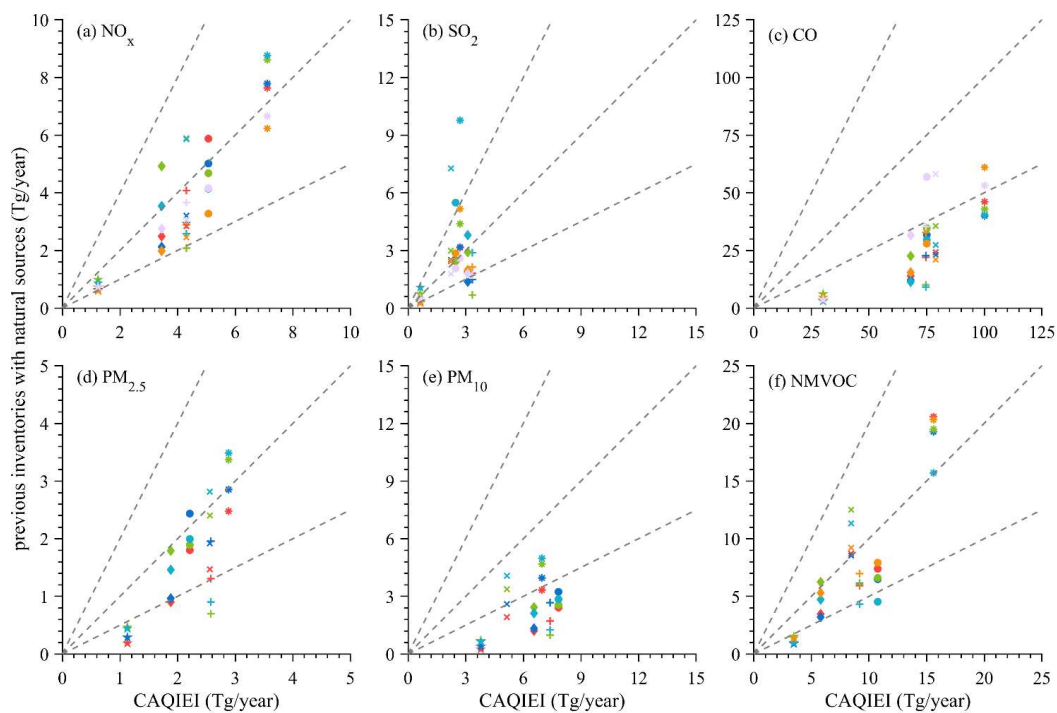
1128



1129

1130 **Figure 10: Comparisons of the averaged emissions of (a) NO_x, (b) SO₂, (c) CO, (d) PM_{2.5}, (e) PM₁₀, and (f) NMVOCs over China**
 1131 **from 2015 to 2018 between CAQIEI and previous inventories added with natural sources.**

1132



1133 ● MEIC ● ABaCAS ● HTAPv3 ● EDGARv6 ● CEDS ● TCR ● NCP ● + NE ● SE ● × SW ● ★ NW ● ◆ Central

1134 **Figure 11: Comparisons of the averaged emissions of (a) NO_x, (b) SO₂, (c) CO, (d) PM_{2.5}, (e) PM₁₀, and (f) NMVOCs over different**
 1135 **regions in China from 2015 to 2018 between CAQIEI and previous inventories added with natural sources.**

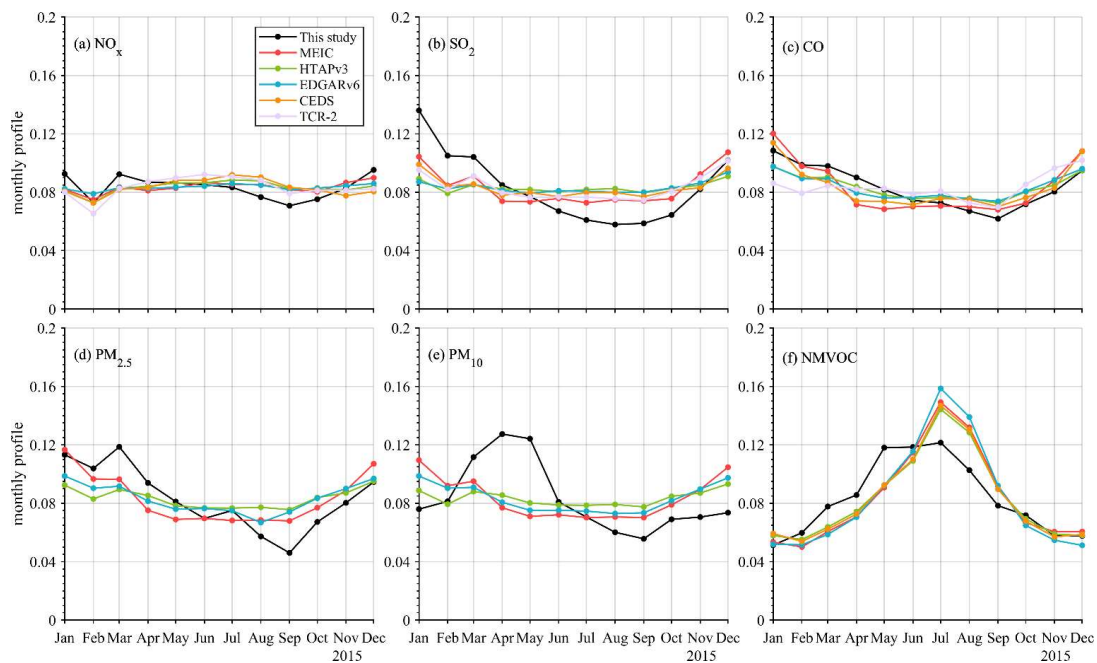
1136

1137

1138

1139

1140



1141

1142 **Figure 12: Comparisons of the monthly profiles of (a) NO_x, (b) SO₂, (c) CO, (d) PM_{2.5}, (e) PM₁₀, and (f) NMVOCs over China in**
1143 **2015 between CAQIEI and previous inventories added with natural sources.**

1144

1145

1146

1147

1148

1149

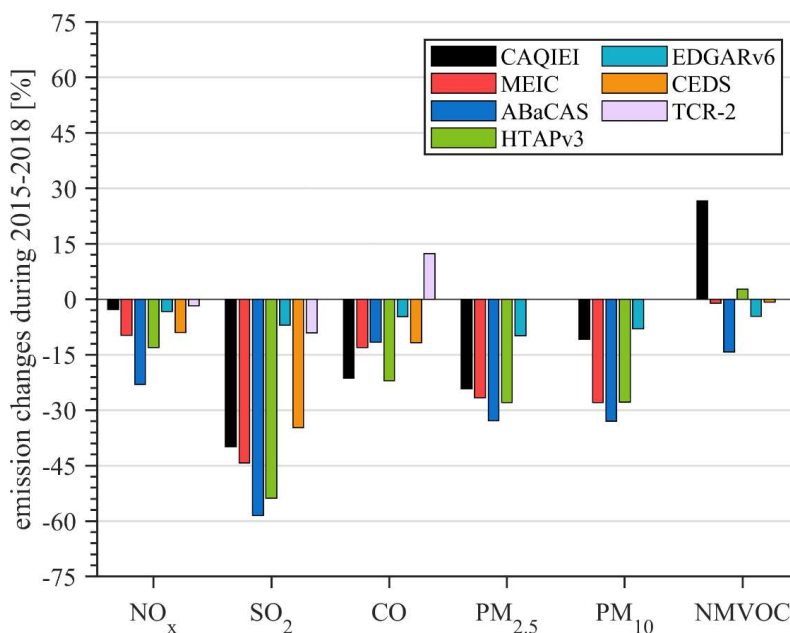
1150

1151

1152

1153

1154



1155

1156 **Figure 13:** Comparisons of the calculated emission changes of (a) NO_x, (b) SO₂, (c) CO, (d) PM_{2.5}, (e) PM₁₀, and (f) NMVOCs over
1157 China from 2015 to 2018 between CAQIEI and previous inventories.

1158 **Author contributions**

1159 X.T., Z.W., and J.Z. conceived and designed the project; L.K., H.W., X.T., and L.W. established the data assimilation system;
1160 Q.W. and L.K. performed the meteorology simulations; L.K., H.C., and J.L. conducted the ensemble simulation with the
1161 NAQPMS model; J.L., L.Z., W.W., B.L., Q.W., D.C. and Y.P. provided the air quality monitoring data; H.W. performed the
1162 quality control of the observation data; and L.K. performed the inversion estimation, generated the figures, and wrote the paper,
1163 with comments provided by G.R.C.

1164 **Competing interests**

1165 The authors declare no competing financial interest.

1166 **Acknowledgements**

1167 We acknowledge the use of surface air quality observation data from CNEMC and the support from the National Key Scientific
1168 and Technological Infrastructure project “Earth System Science Numerical Simulator Facility” (EarthLab).

1169 **Financial support**

1170 This research has been sponsored by the National Natural Science Foundation of China (Grant Nos. 42175132, 92044303,
1171 42205119), the National Key R&D Program (Grant No. 2020YFA0607802), the CAS Information Technology Program (Grant
1172 No. CAS-WX2021SF-0107-02).



1173 References

- 1174 Athanasopoulou, E., Tombrou, M., Pandis, S. N., and Russell, A. G.: The role of sea-salt emissions and heterogeneous chemistry in the air
1175 quality of polluted coastal areas, *Atmos. Chem. Phys.*, 8, 5755-5769, <https://doi.org/10.5194/acp-8-5755-2008>, 2008.
- 1176 Bergamaschi, P., Hein, R., Heimann, M., and Crutzen, P. J.: Inverse modeling of the global CO cycle 1. Inversion of CO mixing ratios, *J.*
1177 *Geophys. Res.-Atmos.*, 105, 1909-1927, <https://doi.org/10.1029/1999jd900818>, 2000.
- 1178 Bobbink, R., Hornung, M., and Roelofs, J. G. M.: The effects of air-borne nitrogen pollutants on species diversity in natural and semi-natural
1179 European vegetation, *J. Ecol.*, 86, 717-738, <https://doi.org/10.1046/j.1365-2745.1998.8650717.x>, 1998.
- 1180 Brasseur, G. P., Hauglustaine, D. A., Walters, S., Rasch, P. J., Müller, J.-F., Granier, C., and Tie, X. X.: MOZART, a global chemical
1181 transport model for ozone and related chemical tracers: 1. Model description, *J. Geophys. Res.-Atmos.*, 103, 28265-28289,
1182 <https://doi.org/10.1029/98JD02397>, 1998.
- 1183 Cohen, A. J., Brauer, M., Burnett, R., Anderson, H. R., Frostad, J., Estep, K., Balakrishnan, K., Brunekreef, B., Dandona, L., Dandona, R.,
1184 Feigin, V., Freedman, G., Hubbell, B., Jobling, A., Kan, H., Knibbs, L., Liu, Y., Martin, R., Morawska, L., Pope, C. A., Shin, H., Straif,
1185 K., Shaddick, G., Thomas, M., van Dingenen, R., van Donkelaar, A., Vos, T., Murray, C. J. L., and Forouzanfar, M. H.: Estimates and
1186 25-year trends of the global burden of disease attributable to ambient air pollution: an analysis of data from the Global Burden of
1187 Diseases Study 2015, *Lancet*, 389, 1907-1918, [https://doi.org/10.1016/s0140-6736\(17\)30505-6](https://doi.org/10.1016/s0140-6736(17)30505-6), 2017.
- 1188 Crippa, M., Guizzardi, D., Butler, T., Keating, T., Wu, R., Kaminski, J., Kuenen, J., Kurokawa, J., Chatani, S., Morikawa, T., Pouliot, G.,
1189 Racine, J., Moran, M. D., Klimont, Z., Manseau, P. M., Mashayekhi, R., Henderson, B. H., Smith, S. J., Suchyta, H., Muntean, M.,
1190 Solazzo, E., Banja, M., Schaaf, E., Pagani, F., Woo, J. H., Kim, J., Monforti-Ferrario, F., Pisoni, E., Zhang, J., Niemi, D., Sassi, M.,
1191 Ansari, T., and Foley, K.: The HTAP_v3 emission mosaic: merging regional and global monthly emissions (2000–2018) to support
1192 air quality modelling and policies, *Earth Syst. Sci. Data*, 15, 2667-2694, <https://doi.org/10.5194/essd-15-2667-2023>, 2023.
- 1193 Dee, D. P. and Da Silva, A. M.: Data assimilation in the presence of forecast bias, *Q. J. R. Meteorol. Soc.*, 124, 269-295,
1194 <https://doi.org/10.1002/qj.49712454512>, 1998.
- 1195 Elbern, H., Strunk, A., Schmidt, H., and Talagrand, O.: Emission rate and chemical state estimation by 4-dimensional variational inversion,
1196 *Atmos. Chem. Phys.*, 7, 3749-3769, <https://doi.org/10.5194/acp-7-3749-2007>, 2007.
- 1197 Elguindi, N., Granier, C., Stavrou, T., Darras, S., Bauwens, M., Cao, H., Chen, C., van der Gon, H., Dubovik, O., Fu, T. M., Henze, D.
1198 K., Jiang, Z., Keita, S., Kuenen, J. J. P., Kurokawa, J., Lioussé, C., Miyazaki, K., Müller, J. F., Qu, Z., Solmon, F., and Zheng, B.:
1199 Intercomparison of Magnitudes and Trends in Anthropogenic Surface Emissions From Bottom-Up Inventories, Top-Down Estimates,
1200 and Emission Scenarios, *Earth Future*, 8, 20, <https://doi.org/10.1029/2020ef001520>, 2020.
- 1201 Evensen, G.: Sequential data assimilation with a nonlinear quasi-geostrophic model using Monte Carlo methods to forecast error statistics,
1202 *J. Geophys. Res.-Oceans*, 99, 10143-10162, <https://doi.org/10.1029/94JC00572>, 1994.
- 1203 Fan, H., Zhao, C., Yang, Y., and Yang, X.: Spatio-Temporal Variations of the PM_{2.5}/PM₁₀ Ratios and Its Application to Air Pollution Type
1204 Classification in China, *Front. Environ. Sci.*, 9, <https://doi.org/10.3389/fenvs.2021.692440>, 2021.
- 1205 Feng, S., Jiang, F., Wu, Z., Wang, H., Ju, W., and Wang, H.: CO Emissions Inferred From Surface CO Observations Over China in December
1206 2013 and 2017, *J. Geophys. Res.-Atmos.*, 125, e2019JD031808, <https://doi.org/10.1029/2019JD031808>, 2020.
- 1207 Fu, X., Wang, T., Gao, J., Wang, P., Liu, Y. M., Wang, S. X., Zhao, B., and Xue, L. K.: Persistent Heavy Winter Nitrate Pollution Driven
1208 by Increased Photochemical Oxidants in Northern China, *Environ. Sci. Technol.*, 54, 3881-3889,
1209 <https://doi.org/10.1021/acs.est.9b07248>, 2020.
- 1210 Gaubert, B., Emmons, L. K., Raeder, K., Tilmes, S., Miyazaki, K., Arellano Jr, A. F., Elguindi, N., Granier, C., Tang, W., Barré, J., Worden,
1211 H. M., Buchholz, R. R., Edwards, D. P., Franke, P., Anderson, J. L., Saunois, M., Schroeder, J., Woo, J. H., Simpson, I. J., Blake, D.
1212 R., Meinardi, S., Wennberg, P. O., Crouse, J., Teng, A., Kim, M., Dickerson, R. R., He, H., Ren, X., Pusede, S. E., and Diskin, G. S.:
1213 Correcting model biases of CO in East Asia: impact on oxidant distributions during KORUS-AQ, *Atmos. Chem. Phys.*, 20, 14617-
1214 14647, <https://doi.org/10.5194/acp-20-14617-2020>, 2020.
- 1215 Granier, C., Lamarque, J., Mieville, A., Müller, J., Olivier, J., Orlando, J., Peters, J., Petron, G., Tyndall, G., and Wallens, S.: POET, a
1216 database of surface emissions of ozone precursors, available at: <http://www.aero.jussieu.fr/projet/ACCENT/POET.php> (last access: 09
1217 October 2023), 2005.



- 1218 Hauglustaine, D. A., Brasseur, G. P., Walters, S., Rasch, P. J., Muller, J. F., Emmons, L. K., and Carroll, C. A.: MOZART, a global chemical
1219 transport model for ozone and related chemical tracers 2. Model results and evaluation, *J. Geophys. Res.-Atmos.*, 103, 28291-28335,
1220 <https://doi.org/10.1029/98jd02398>, 1998.
- 1221 Henze, D. K., Seinfeld, J. H., and Shindell, D. T.: Inverse modeling and mapping US air quality influences of inorganic PM_{2.5} precursor
1222 emissions using the adjoint of GEOS-Chem, *Atmos. Chem. Phys.*, 9, 5877-5903, <https://doi.org/10.5194/acp-9-5877-2009>, 2009.
- 1223 Hernández, D. L., Vallano, D. M., Zavaleta, E. S., Tzankova, Z., Pasari, J. R., Weiss, S., Selmants, P. C., and Morozumi, C.: Nitrogen
1224 Pollution Is Linked to US Listed Species Declines, *BioScience*, 66, 213-222, <https://doi.org/10.1093/biosci/biw003>, 2016.
- 1225 Jalkanen, J. P., Johansson, L., Kukkonen, J., Brink, A., Kalli, J., and Stipa, T.: Extension of an assessment model of ship traffic exhaust
1226 emissions for particulate matter and carbon monoxide, *Atmos. Chem. Phys.*, 12, 2641-2659, <https://doi.org/10.5194/acp-12-2641-2012>,
1227 2012.
- 1228 Janssens-Maenhout, G., Crippa, M., Guizzardi, D., Dentener, F., Muntean, M., Pouliot, G., Keating, T., Zhang, Q., Kurokawa, J.,
1229 Wankmuller, R., van der Gon, H. D., Kuenen, J. J. P., Klimont, Z., Frost, G., Darras, S., Koffi, B., and Li, M.: HTAP_v2.2: a mosaic
1230 of regional and global emission grid maps for 2008 and 2010 to study hemispheric transport of air pollution, *Atmos. Chem. Phys.*, 15,
1231 11411-11432, <https://doi.org/10.5194/acp-15-11411-2015>, 2015.
- 1232 Jiang, Z., Worden, J. R., Worden, H., Deeter, M., Jones, D. B. A., Arellano, A. F., and Henze, D. K.: A 15-year record of CO emissions
1233 constrained by MOPITT CO observations, *Atmos. Chem. Phys.*, 17, 4565-4583, <https://doi.org/10.5194/acp-17-4565-2017>, 2017.
- 1234 Kaiser, J. W., Heil, A., Andreae, M. O., Benedetti, A., Chubarova, N., Jones, L., Morcrette, J. J., Razinger, M., Schultz, M. G., Suttie, M.,
1235 and van der Werf, G. R.: Biomass burning emissions estimated with a global fire assimilation system based on observed fire radiative
1236 power, *Biogeosciences*, 9, 527-554, <https://doi.org/10.5194/bg-9-527-2012>, 2012.
- 1237 Kan, H., Chen, R., and Tong, S.: Ambient air pollution, climate change, and population health in China, *Environ. Int.*, 42, 10-19,
1238 <https://doi.org/10.1016/j.envint.2011.03.003>, 2012.
- 1239 Kong, L., Tang, X., Wang, Z. F., Zhu, J., Li, J. J., Wu, H. J., Wu, Q. Z., Chen, H. S., Zhu, L. L., Wang, W., Liu, B., Wang, Q., Chen D. H.,
1240 Pan Y. P., Li, J., Wu, L., and Carmichael, G. R.: Inversed Emission Inventory for Chinese Air Quality (CAQIEI) version 1.0, *Science*
1241 *Data Bank* [dataset], <https://doi.org/10.57760/sciencedb.13151>, 2023.
- 1242 Kong, L., Tang, X., Zhu, J., Wang, Z., Pan, Y., Wu, H., Wu, L., Wu, Q., He, Y., Tian, S., Xie, Y., Liu, Z., Sui, W., Han, L., and Carmichael,
1243 G.: Improved Inversion of Monthly Ammonia Emissions in China Based on the Chinese Ammonia Monitoring Network and Ensemble
1244 Kalman Filter, *Environ. Sci. Technol.*, 53, 12529-12538, <https://doi.org/10.1021/acs.est.9b02701>, 2019.
- 1245 Kong, L., Tang, X., Zhu, J., Wang, Z., Sun, Y., Fu, P., Gao, M., Wu, H., Lu, M., Wu, Q., Huang, S., Sui, W., Li, J., Pan, X., Wu, L., Akimoto,
1246 H., and Carmichael, G. R.: Unbalanced emission reductions of different species and sectors in China during COVID-19 lockdown
1247 derived by multi-species surface observation assimilation, *Atmos. Chem. Phys.*, 23, 6217-6240, <https://doi.org/10.5194/acp-23-6217-2023>,
1248 2023.
- 1249 Kong, L., Tang, X., Zhu, J., Wang, Z., Li, J., Wu, H., Wu, Q., Chen, H., Zhu, L., Wang, W., Liu, B., Wang, Q., Chen, D., Pan, Y., Song, T.,
1250 Li, F., Zheng, H., Jia, G., Lu, M., Wu, L., and Carmichael, G. R.: A 6-year-long (2013–2018) high-resolution air quality reanalysis
1251 dataset in China based on the assimilation of surface observations from CNEMC, *Earth Syst. Sci. Data*, 13, 529-570,
1252 <https://doi.org/10.5194/essd-13-529-2021>, 2021.
- 1253 Kong, L., Tang, X., Zhu, J., Wang, Z., Fu, J. S., Wang, X., Itahashi, S., Yamaji, K., Nagashima, T., Lee, H. J., Kim, C. H., Lin, C. Y., Chen,
1254 L., Zhang, M., Tao, Z., Li, J., Kajino, M., Liao, H., Wang, Z., Sudo, K., Wang, Y., Pan, Y., Tang, G., Li, M., Wu, Q., Ge, B., and
1255 Carmichael, G. R.: Evaluation and uncertainty investigation of the NO₂, CO and NH₃ modeling over China under the framework of
1256 MICS-Asia III, *Atmos. Chem. Phys.*, 20, 181-202, <https://doi.org/10.5194/acp-20-181-2020>, 2020.
- 1257 Koohkan, M. R., Bocquet, M., Roustan, Y., Kim, Y., and Seigneur, C.: Estimation of volatile organic compound emissions for Europe using
1258 data assimilation, *Atmos. Chem. Phys.*, 13, 5887-5905, <https://doi.org/10.5194/acp-13-5887-2013>, 2013.
- 1259 Koukouli, M. E., Theys, N., Ding, J. Y., Zyrichidou, I., Mijling, B., Balis, D., and Johannes, V. R.: Updated SO₂ emission estimates over
1260 China using OMI/Aura observations, *Atmos. Meas. Tech.*, 11, 1817-1832, [10.5194/amt-11-1817-2018](https://doi.org/10.5194/amt-11-1817-2018), 2018.
- 1261 Krotkov, N. A., McLinden, C. A., Li, C., Lamsal, L. N., Celarier, E. A., Marchenko, S. V., Swartz, W. H., Bucsela, E. J., Joiner, J., Duncan,
1262 B. N., Boersma, K. F., Veefkind, J. P., Levelt, P. F., Fioletov, V. E., Dickerson, R. R., He, H., Lu, Z. F., and Streets, D. G.: Aura OMI
1263 observations of regional SO₂ and NO₂ pollution changes from 2005 to 2015, *Atmos. Chem. Phys.*, 16, 4605-4629,
1264 <https://doi.org/10.5194/acp-16-4605-2016>, 2016.



- 1265 Krupa, S. V.: Effects of atmospheric ammonia (NH₃) on terrestrial vegetation: a review, *Environ. Pollut.*, 124, 179-221,
1266 [https://doi.org/10.1016/s0269-7491\(02\)00434-7](https://doi.org/10.1016/s0269-7491(02)00434-7), 2003.
- 1267 Kurokawa, J. and Ohara, T.: Long-term historical trends in air pollutant emissions in Asia: Regional Emission inventory in ASia (REAS)
1268 version 3, *Atmos. Chem. Phys.*, 20, 12761-12793, <https://doi.org/10.5194/acp-20-12761-2020>, 2020.
- 1269 Kurokawa, J., Ohara, T., Morikawa, T., Hanayama, S., Janssens-Maenhout, G., Fukui, T., Kawashima, K., and Akimoto, H.: Emissions of
1270 air pollutants and greenhouse gases over Asian regions during 2000-2008: Regional Emission inventory in ASia (REAS) version 2,
1271 *Atmos. Chem. Phys.*, 13, 11019-11058, <https://doi.org/10.5194/acp-13-11019-2013>, 2013.
- 1272 Lei, L., Zhou, W., Chen, C., He, Y., Li, Z. J., Sun, J. X., Tang, X., Fu, P. Q., Wang, Z. F., and Sun, Y. L.: Long-term characterization of
1273 aerosol chemistry in cold season from 2013 to 2020 in Beijing, China, *Environ. Pollut.*, 268, 9, [10.1016/j.envpol.2020.115952](https://doi.org/10.1016/j.envpol.2020.115952), 2021.
- 1274 Li, C., McLinden, C., Fioletov, V., Krotkov, N., Carn, S., Joiner, J., Streets, D., He, H., Ren, X., Li, Z., and Dickerson, R. R.: India Is
1275 Overtaking China as the World's Largest Emitter of Anthropogenic Sulfur Dioxide, *Sci Rep*, 7, 14304, <https://doi.org/10.1038/s41598-017-14639-8>, 2017a.
- 1277 Li, H., Cheng, J., Zhang, Q., Zheng, B., Zhang, Y., Zheng, G., and He, K.: Rapid transition in winter aerosol composition in Beijing from
1278 2014 to 2017: response to clean air actions, *Atmos. Chem. Phys.*, 19, 11485-11499, <https://doi.org/10.5194/acp-19-11485-2019>, 2019a.
- 1279 Li, J., Wang, Z., Zhuang, G., Luo, G., Sun, Y., and Wang, Q.: Mixing of Asian mineral dust with anthropogenic pollutants over East Asia:
1280 a model case study of a super-duststorm in March 2010, *Atmos. Chem. Phys.*, 12, 7591-7607, 2012.
- 1281 Li, K., Jacob, D. J., Liao, H., Shen, L., Zhang, Q., and Bates, K. H.: Anthropogenic drivers of 2013-2017 trends in summer surface ozone in
1282 China, *Proc. Natl. Acad. Sci. U.S.A.*, 116, 422-427, <https://doi.org/10.1073/pnas.1812168116>, 2019b.
- 1283 Li, L. Y., Yang, W. Z., Xie, S. D., and Wu, Y.: Estimations and uncertainty of biogenic volatile organic compound emission inventory in
1284 China for 2008-2018, *Sci. Total Environ.*, 733, 10, <https://doi.org/10.1016/j.scitotenv.2020.139301>, 2020a.
- 1285 Li, M., Zhang, Q., Zheng, B., Tong, D., Lei, Y., Liu, F., Hong, C. P., Kang, S. C., Yan, L., Zhang, Y. X., Bo, Y., Su, H., Cheng, Y. F., and
1286 He, K. B.: Persistent growth of anthropogenic non-methane volatile organic compound (NMVOC) emissions in China during 1990-
1287 2017: drivers, speciation and ozone formation potential, *Atmos. Chem. Phys.*, 19, 8897-8913, <https://doi.org/10.5194/acp-19-8897-2019>, 2019c.
- 1289 Li, M., Zhang, Q., Kurokawa, J. I., Woo, J. H., He, K., Lu, Z., Ohara, T., Song, Y., Streets, D. G., Carmichael, G. R., Cheng, Y., Hong, C.,
1290 Huo, H., Jiang, X., Kang, S., Liu, F., Su, H., and Zheng, B.: MIX: a mosaic Asian anthropogenic emission inventory under the
1291 international collaboration framework of the MICS-Asia and HTAP, *Atmos. Chem. Phys.*, 17, 935-963, <https://doi.org/10.5194/acp-17-935-2017>, 2017b.
- 1293 Li, N., Long, X., Tie, X. X., Cao, J. J., Huang, R. J., Zhang, R., Feng, T., Liu, S. X., and Li, G. H.: Urban dust in the Guanzhong basin of
1294 China, part II: A case study of urban dust pollution using the WRF-Dust model, *Sci. Total Environ.*, 541, 1614-1624,
1295 <https://doi.org/10.1016/j.scitotenv.2015.10.028>, 2016.
- 1296 Li, R., Cui, L. L., Li, J. L., Zhao, A., Fu, H. B., Wu, Y., Zhang, L. W., Kong, L. D., and Chen, J. M.: Spatial and temporal variation of
1297 particulate matter and gaseous pollutants in China during 2014-2016, *Atmos. Environ.*, 161, 235-246,
1298 <https://doi.org/10.1016/j.atmosenv.2017.05.008>, 2017c.
- 1299 Li, S., Wang, S., Wu, Q., Zhang, Y., Ouyang, D., Zheng, H., Han, L., Qiu, X., Wen, Y., Liu, M., Jiang, Y., Yin, D., Liu, K., Zhao, B., Zhang,
1300 S., Wu, Y., and Hao, J.: Emission trends of air pollutants and CO₂ in China from 2005 to 2021, *Earth Syst. Sci. Data*, 15, 2279-2294,
1301 <https://doi.org/10.5194/essd-15-2279-2023>, 2023.
- 1302 Li, W., Shao, L., Wang, W., Li, H., Wang, X., Li, Y., Li, W., Jones, T., and Zhang, D.: Air quality improvement in response to intensified
1303 control strategies in Beijing during 2013-2019, *Sci. Total Environ.*, 744, <https://doi.org/10.1016/j.scitotenv.2020.140776>, 2020b.
- 1304 Liu, J., Tong, D., Zheng, Y. X., Cheng, J., Qin, X. Y., Shi, Q. R., Yan, L., Lei, Y., and Zhang, Q.: Carbon and air pollutant emissions from
1305 China's cement industry 1990-2015: trends, evolution of technologies, and drivers, *Atmos. Chem. Phys.*, 21, 1627-1647,
1306 <https://doi.org/10.5194/acp-21-1627-2021>, 2021.
- 1307 Liu, J., Mauzerall, D. L., Chen, Q., Zhang, Q., Song, Y., Peng, W., Klimont, Z., Qiu, X. H., Zhang, S. Q., Hu, M., Lin, W. L., Smith, K. R.,
1308 and Zhu, T.: Air pollutant emissions from Chinese households: A major and underappreciated ambient pollution source, *Proc. Natl.
1309 Acad. Sci. U.S.A.*, 113, 7756-7761, <https://doi.org/10.1073/pnas.1604537113>, 2016.
- 1310 Lu, X., Zhang, L., Wang, X. L., Gao, M., Li, K., Zhang, Y. Z., Yue, X., and Zhang, Y. H.: Rapid Increases in Warm-Season Surface Ozone
1311 and Resulting Health Impact in China Since 2013, *Environ. Sci. Technol. Lett.*, 7, 240-247, <https://doi.org/10.1021/acs.estlett.0c00171>,
1312 2020.



- 1313 Lu, X., Hong, J. Y., Zhang, L., Cooper, O. R., Schultz, M. G., Xu, X. B., Wang, T., Gao, M., Zhao, Y. H., and Zhang, Y. H.: Severe Surface
1314 Ozone Pollution in China: A Global Perspective, *Environ. Sci. Technol. Lett.*, 5, 487-494, <https://doi.org/10.1021/acs.estlett.8b00366>,
1315 2018.
- 1316 Ma, C. Q., Wang, T. J., Mizzi, A. P., Anderson, J. L., Zhuang, B. L., Xie, M., and Wu, R. S.: Multiconstituent Data Assimilation With WRF-
1317 Chem/DART: Potential for Adjusting Anthropogenic Emissions and Improving Air Quality Forecasts Over Eastern China, *J. Geophys.*
1318 *Res.-Atmos.*, 124, 7393-7412, <https://doi.org/10.1029/2019jd030421>, 2019.
- 1319 Martin, S. T., Hung, H. M., Park, R. J., Jacob, D. J., Spurr, R. J. D., Chance, K. V., and Chin, M.: Effects of the physical state of tropospheric
1320 ammonium-sulfate-nitrate particles on global aerosol direct radiative forcing, *Atmos. Chem. Phys.*, 4, 183-214,
1321 <https://doi.org/10.5194/acp-4-183-2004>, 2004.
- 1322 McDuffie, E. E., Smith, S. J., O'Rourke, P., Tibrewal, K., Venkataraman, C., Marais, E. A., Zheng, B., Crippa, M., Brauer, M., and Martin,
1323 R. V.: A global anthropogenic emission inventory of atmospheric pollutants from sector- and fuel-specific sources (1970-2017): an
1324 application of the Community Emissions Data System (CEDS), *Earth Syst. Sci. Data*, 12, 3413-3442, <https://doi.org/10.5194/essd-12-3413-2020>, 2020.
- 1326 Miyazaki, K. and Eskes, H.: Constraints on surface NOx emissions by assimilating satellite observations of multiple species, *Geophys. Res.*
1327 *Let.*, 40, 4745-4750, <https://doi.org/10.1002/grl.50894>, 2013.
- 1328 Miyazaki, K., Bowman, K. W., Yumimoto, K., Walker, T., and Sudo, K.: Evaluation of a multi-model, multi-constituent assimilation
1329 framework for tropospheric chemical reanalysis, *Atmos. Chem. Phys.*, 20, 931-967, <https://doi.org/10.5194/acp-20-931-2020>, 2020a.
- 1330 Miyazaki, K., Eskes, H. J., Sudo, K., Takigawa, M., van Weele, M., and Boersma, K. F.: Simultaneous assimilation of satellite NO₂, O₃,
1331 CO, and HNO₃ data for the analysis of tropospheric chemical composition and emissions, *Atmos. Chem. Phys.*, 12, 9545-9579,
1332 <https://doi.org/10.5194/acp-12-9545-2012>, 2012.
- 1333 Miyazaki, K., Bowman, K., Sekiya, T., Eskes, H., Boersma, F., Worden, H., Livesey, N., Payne, V. H., Sudo, K., Kanaya, Y., Takigawa,
1334 M., and Ogochi, K.: Updated tropospheric chemistry reanalysis and emission estimates, TCR-2, for 2005–2018, *Earth Syst. Sci. Data*,
1335 12, 2223-2259, <https://doi.org/10.5194/essd-12-2223-2020>, 2020b.
- 1336 Müller, J.-F., Stavrou, T., Bauwens, M., George, M., Hurtmans, D., Coheur, P.-F., Clerbaux, C., and Sweeney, C.: Top-Down CO
1337 Emissions Based On IASI Observations and Hemispheric Constraints on OH Levels, *Geophys. Res. Lett.*, 45, 1621-1629,
1338 <https://doi.org/10.1002/2017GL076697>, 2018.
- 1339 Muller, J. F., Stavrou, T., Bauwens, M., George, M., Hurtmans, D., Coheur, P. F., Clerbaux, C., and Sweeney, C.: Top-Down CO
1340 Emissions Based On IASI Observations and Hemispheric Constraints on OH Levels, *Geophys. Res. Lett.*, 45, 1621-1629,
1341 <https://doi.org/10.1002/2017gl076697>, 2018.
- 1342 Paulot, F., Jacob, D. J., Pinder, R. W., Bash, J. O., Travis, K., and Henze, D. K.: Ammonia emissions in the United States, European Union,
1343 and China derived by high-resolution inversion of ammonium wet deposition data: Interpretation with a new agricultural emissions
1344 inventory (MASAGE_NH3), *J. Geophys. Res.-Atmos.*, 119, 4343-4364, <https://doi.org/10.1002/2013jd021130>, 2014.
- 1345 Peng, Z., Lei, L., Tan, Z. M., Zhang, M., Ding, A., and Kou, X.: Dynamics-based estimates of decline trend with fine temporal variations in
1346 China's PM_{2.5} emissions, *EGUsphere*, 2023, 1-34, <https://doi.org/10.5194/egusphere-2023-755>, 2023.
- 1347 Peng, Z., Lei, L. L., Liu, Z. Q., Su, J. N., Ding, A. J., Ban, J. M., Chen, D., Kou, X. X., and Chu, K. K.: The impact of multi-species surface
1348 chemical observation assimilation on air quality forecasts in China, *Atmos. Chem. Phys.*, 18, 18, [https://doi.org/10.5194/acp-18-17387-](https://doi.org/10.5194/acp-18-17387-2018)
1349 2018, 2018.
- 1350 Petron, G., Granier, C., Khattatov, B., Lamarque, J. F., Yudin, V., Muller, J. F., and Gille, J.: Inverse modeling of carbon monoxide surface
1351 emissions using Climate Monitoring and Diagnostics Laboratory network observations, *J. Geophys. Res.-Atmos.*, 107, 23,
1352 <https://doi.org/10.1029/2001jd001305>, 2002.
- 1353 Petron, G., Granier, C., Khattatov, B., Yudin, V., Lamarque, J. F., Emmons, L., Gille, J., and Edwards, D. P.: Monthly CO surface sources
1354 inventory based on the 2000-2001 MOPITT satellite data, *Geophys. Res. Lett.*, 31, 5, <https://doi.org/10.1029/2004gl020560>, 2004.
- 1355 Philip, S., Martin, R. V., Snider, G., Weagle, C. L., van Donkelaar, A., Brauer, M., Henze, D. K., Klimont, Z., Venkataraman, C., Gutikunda,
1356 S. K., and Zhang, Q.: Anthropogenic fugitive, combustion and industrial dust is a significant, underrepresented fine particulate matter
1357 source in global atmospheric models, *Environ. Res. Lett.*, 12, 7, <https://doi.org/10.1088/1748-9326/aa65a4>, 2017.
- 1358 Price, C., Penner, J., and Prather, M.: NO_x from lightning .1. Global distribution based on lightning physics, *J. Geophys. Res.-Atmos.*, 102,
1359 5929-5941, <https://doi.org/10.1029/96jd03504>, 1997.



- 1360 Prospero, J. M., Ginoux, P., Torres, O., Nicholson, S. E., and Gill, T. E.: Environmental characterization of global sources of atmospheric
1361 soil dust identified with the Nimbus 7 Total Ozone Mapping Spectrometer (TOMS) absorbing aerosol product, *Rev. Geophys.*, 40, 31,
1362 <https://doi.org/10.1029/2000rg000095>, 2002.
- 1363 Qu, Z., Henze, D. K., Capps, S. L., Wang, Y., Xu, X. G., Wang, J., and Keller, M.: Monthly top-down NO_x emissions for China (2005-2012):
1364 A hybrid inversion method and trend analysis, *J. Geophys. Res.-Atmos.*, 122, 4600-4625, <https://doi.org/10.1002/2016jd025852>, 2017.
- 1365 Qu, Z., Henze, D. K., Li, C., Theys, N., Wang, Y., Wang, J., Wang, W., Han, J., Shim, C., Dickerson, R. R., and Ren, X. R.: SO₂ Emission
1366 Estimates Using OMI SO₂ Retrievals for 2005-2017, *J. Geophys. Res.-Atmos.*, 124, 8336-8359, <https://doi.org/10.1029/2019jd030243>,
1367 2019.
- 1368 Randerson, J. T., Van Der Werf, G. R., Giglio, L., Collatz, G. J., and Kasibhatla, P. S.: Global Fire Emissions Database, Version 4.1
1369 (GFEDv4), ORNL DAAC, Oak Ridge, Tennessee, USA, <https://doi.org/10.3334/ORNLDAAC/1293>, 2017.
- 1370 Sakov, P. and Oke, P. R.: A deterministic formulation of the ensemble Kalman filter: an alternative to ensemble square root filters, *Tellus*
1371 *Ser. A-Dyn. Meteorol. Oceanol.*, 60, 361-371, <https://doi.org/10.1111/j.1600-0870.2007.00299.x>, 2008.
- 1372 Sindelarova, K., Granier, C., Bouarar, I., Guenther, A., Tilmes, S., Stavrou, T., Muller, J. F., Kuhn, U., Stefani, P., and Knorr, W.: Global
1373 data set of biogenic VOC emissions calculated by the MEGAN model over the last 30 years, *Atmos. Chem. Phys.*, 14, 9317-9341,
1374 <https://doi.org/10.5194/acp-14-9317-2014>, 2014.
- 1375 Song, C., Wu, L., Xie, Y., He, J., Chen, X., Wang, T., Lin, Y., Jin, T., Wang, A., Liu, Y., Dai, Q., Liu, B., Wang, Y.-n., and Mao, H.: Air
1376 pollution in China: Status and spatiotemporal variations, *Environ. Pollut.*, 227, 334-347, <https://doi.org/10.1016/j.envpol.2017.04.075>,
1377 2017.
- 1378 Stein, O., Schultz, M. G., Bouarar, I., Clark, H., Huijnen, V., Gaudel, A., George, M., and Clerbaux, C.: On the wintertime low bias of
1379 Northern Hemisphere carbon monoxide found in global model simulations, *Atmos. Chem. Phys.*, 14, 9295-9316,
1380 <https://doi.org/10.5194/acp-14-9295-2014>, 2014.
- 1381 Streets, D. G., Bond, T. C., Carmichael, G. R., Fernandes, S. D., Fu, Q., He, D., Klimont, Z., Nelson, S. M., Tsai, N. Y., Wang, M. Q., Woo,
1382 J. H., and Yarber, K. F.: An inventory of gaseous and primary aerosol emissions in Asia in the year 2000, *J. Geophys. Res.-Atmos.*,
1383 108, n/a-n/a, <https://doi.org/10.1029/2002JD003093>, 2003.
- 1384 Tandeo, P., Ailliot, P., Bocquet, M., Carrassi, A., Miyoshi, T., Pulido, M., and Zhen, Y. C.: A Review of Innovation-Based Methods to
1385 Jointly Estimate Model and Observation Error Covariance Matrices in Ensemble Data Assimilation, *Mon. Weather Rev.*, 148, 3973-
1386 3994, <https://doi.org/10.1175/mwr-d-19-0240.1>, 2020.
- 1387 Tang, M., Liu, Y., He, J., Wang, Z., Wu, Z., and Ji, D.: In situ continuous hourly observations of wintertime nitrate, sulfate and ammonium
1388 in a megacity in the North China plain from 2014 to 2019: Temporal variation, chemical formation and regional transport,
1389 *Chemosphere*, 262, <https://doi.org/10.1016/j.chemosphere.2020.127745>, 2021.
- 1390 Tang, X., Zhu, J., Wang, Z., Gbaguidi, A., Lin, C., Xin, J., Song, T., and Hu, B.: Limitations of ozone data assimilation with adjustment of
1391 NO_x emissions: mixed effects on NO₂ forecasts over Beijing and surrounding areas, *Atmos. Chem. Phys.*, 16, 6395-6405,
1392 <https://doi.org/10.5194/acp-16-6395-2016>, 2016.
- 1393 Tang, X., Zhu, J., Wang, Z., Wang, M., Gbaguidi, A., Li, J., Shao, M., Tang, G. Q., and Ji, D. S.: Inversion of CO emissions over Beijing
1394 and its surrounding areas with ensemble Kalman filter, *Atmos. Environ.*, 81, 676-686, <https://doi.org/10.1016/j.atmosenv.2013.08.051>,
1395 2013.
- 1396 Tegen, I., Lacis, A. A., and Fung, I.: The influence on climate forcing of mineral aerosols from disturbed soils, *Nature*, 380, 419-422,
1397 <https://doi.org/10.1038/380419a0>, 1996.
- 1398 van der Werf, G. R., Randerson, J. T., Giglio, L., Collatz, G. J., Mu, M., Kasibhatla, P. S., Morton, D. C., DeFries, R. S., Jin, Y., and van
1399 Leeuwen, T. T.: Global fire emissions and the contribution of deforestation, savanna, forest, agricultural, and peat fires (1997-2009),
1400 *Atmos. Chem. Phys.*, 10, 11707-11735, <https://doi.org/10.5194/acp-10-11707-2010>, 2010.
- 1401 von Schneidmesser, E., Monks, P. S., Allan, J. D., Bruhwiler, L., Forster, P., Fowler, D., Lauer, A., Morgan, W. T., Paasonen, P., Righi,
1402 M., Sindelarova, K., and Sutton, M. A.: Chemistry and the Linkages between Air Quality and Climate Change, *Chem. Rev.*, 115, 3856-
1403 3897, <https://doi.org/10.1021/acs.chemrev.5b00089>, 2015.
- 1404 Wang, S., Su, H., Chen, C., Tao, W., Streets, D. G., Lu, Z., Zheng, B., Carmichael, G. R., Lelieveld, J., Poeschl, U., and Cheng, Y.: Natural
1405 gas shortages during the "coal-to-gas" transition in China have caused a large redistribution of air pollution in winter 2017, *Proc. Natl.*
1406 *Acad. Sci. U.S.A.*, 117, 31018-31025, <https://doi.org/10.1073/pnas.2007513117>, 2020a.



- 1407 Wang, S. S., Yu, Y., Zhang, X. X., Lu, H. Y., Zhang, X. Y., and Xu, Z. W.: Weakened dust activity over China and Mongolia from 2001 to
1408 2020 associated with climate change and land-use management, *Environ. Res. Lett.*, 16, 12, <https://doi.org/10.1088/1748-9326/ac3b79>,
1409 2021.
- 1410 Wang, X. G. and Bishop, C. H.: A comparison of breeding and ensemble transform Kalman filter ensemble forecast schemes, *J. Atmos. Sci.*,
1411 60, 1140-1158, [https://doi.org/10.1175/1520-0469\(2003\)060<1140:Acobae>2.0.Co;2](https://doi.org/10.1175/1520-0469(2003)060<1140:Acobae>2.0.Co;2), 2003.
- 1412 Wang, X. Y., Lei, Y., Yan, L., Liu, T., Zhang, Q., and He, K. B.: A unit-based emission inventory of SO₂, NO_x and PM for the Chinese
1413 iron and steel industry from 2010 to 2015, *Sci. Total Environ.*, 676, 18-30, <https://doi.org/10.1016/j.scitotenv.2019.04.241>, 2019a.
- 1414 Wang, Y. C., Li, X., Wang, Q. Y., Zhou, B. H., Liu, S. X., Tian, J., Hao, Q., Li, G. H., Han, Y. M., Ho, S. S. H., and Cao, J. J.: Response of
1415 aerosol composition to the clean air actions in Baoji city of Fen-Wei River Basin, *Environ. Res.*, 210, 10,
1416 <https://doi.org/10.1016/j.envres.2022.112936>, 2022.
- 1417 Wang, Y. H., Gao, W. K., Wang, S., Song, T., Gong, Z. Y., Ji, D. S., Wang, L. L., Liu, Z. R., Tang, G. Q., Huo, Y. F., Tian, S. L., Li, J. Y.,
1418 Li, M. G., Yang, Y., Chu, B. W., Petaja, T., Kerminen, V. M., He, H., Hao, J. M., Kulmala, M., Wang, Y. S., and Zhang, Y. H.:
1419 Contrasting trends of PM_{2.5} and surface-ozone concentrations in China from 2013 to 2017, *Natl. Sci. Rev.*, 7, 1331-1339,
1420 <https://doi.org/10.1093/nsr/nwaa032>, 2020b.
- 1421 Wang, Y. S., Li, W. J., Gao, W. K., Liu, Z. R., Tian, S. L., Shen, R. R., Ji, D. S., Wang, S., Wang, L. L., Tang, G. Q., Song, T., Cheng, M.
1422 T., Wang, G. H., Gong, Z. Y., Hao, J. M., and Zhang, Y. H.: Trends in particulate matter and its chemical compositions in China from
1423 2013-2017, *Sci. China-Earth Sci.*, 62, 1857-1871, <https://doi.org/10.1007/s11430-018-9373-1>, 2019b.
- 1424 Wu, C. L., Lin, Z. H., Shao, Y. P., Liu, X. H., and Li, Y.: Drivers of recent decline in dust activity over East Asia, *Nat. Commun.*, 13, 10,
1425 <https://doi.org/10.1038/s41467-022-34823-3>, 2022.
- 1426 World Health Organization (WHO): Ambient air pollution: a global assessment of exposure and burden of disease,
1427 <https://www.who.int/publications/i/item/9789241511353>, last access: 16 November 2023.
- 1428 Wu, H., Tang, X., Wang, Z., Wu, L., Li, J., Wang, W., Yang, W., and Zhu, J.: High-spatiotemporal-resolution inverse estimation of CO and
1429 NO_x emission reductions during emission control periods with a modified ensemble Kalman filter, *Atmos. Environ.*, 236, 117631,
1430 <https://doi.org/10.1016/j.atmosenv.2020.117631>, 2020a.
- 1431 Wu, H. J., Tang, X., Wang, Z. F., Wu, L., Lu, M. M., Wei, L. F., and Zhu, J.: Probabilistic Automatic Outlier Detection for Surface Air
1432 Quality Measurements from the China National Environmental Monitoring Network, *Adv. Atmos. Sci.*, 35, 1522-1532,
1433 <https://doi.org/10.1007/s00376-018-8067-9>, 2018.
- 1434 Wu, J., Kong, S. F., Wu, F. Q., Cheng, Y., Zheng, S. R., Qin, S., Liu, X., Yan, Q., Zheng, H., Zheng, M. M., Yan, Y. Y., Liu, D. T., Ding,
1435 S., Zhao, D. L., Shen, G. F., Zhao, T. L., and Qi, S. H.: The moving of high emission for biomass burning in China: View from multi-
1436 year emission estimation and human-driven forces, *Environ. Int.*, 142, 17, <https://doi.org/10.1016/j.envint.2020.105812>, 2020b.
- 1437 Xu, Q., Wang, S., Jiang, J., Bhattacharai, N., Li, X., Chang, X., Qiu, X., Zheng, M., Hua, Y., and Hao, J.: Nitrate dominates the chemical
1438 composition of PM_{2.5} during haze event in Beijing, China, *Sci. Total Environ.*, 689, 1293-1303,
1439 <https://doi.org/10.1016/j.scitotenv.2019.06.294>, 2019a.
- 1440 Xu, W., Sun, Y., Wang, Q., Zhao, J., Wang, J., Ge, X., Xie, C., Zhou, W., Du, W., Li, J., Fu, P., Wang, Z., Worsnop, D. R., and Coe, H.:
1441 Changes in Aerosol Chemistry From 2014 to 2016 in Winter in Beijing: Insights From High-Resolution Aerosol Mass Spectrometry,
1442 *J. Geophys. Res.-Atmos.*, 124, 1132-1147, <https://doi.org/10.1029/2018JD029245>, 2019b.
- 1443 Xu, Y., Huang, Z., Ye, J., and Zheng, J.: Hourly emissions of air pollutants and greenhouse gases from open biomass burning in China
1444 during 2016–2020, *Sci. Data*, 10, 629, <https://doi.org/10.1038/s41597-023-02541-0>, 2023.
- 1445 Yan, X. Y., Akimoto, H., and Ohara, T.: Estimation of nitrous oxide, nitric oxide and ammonia emissions from croplands in East, Southeast
1446 and South Asia, *Glob. Change Biol.*, 9, 1080-1096, <https://doi.org/10.1046/j.1365-2486.2003.00649.x>, 2003.
- 1447 Yin, L., Du, P., Zhang, M., Liu, M., Xu, T., and Song, Y.: Estimation of emissions from biomass burning in China (2003–2017) based on
1448 MODIS fire radiative energy data, *Biogeosciences*, 16, 1629-1640, <https://doi.org/10.5194/bg-16-1629-2019>, 2019.
- 1449 Zeng, Y., Wang, M., Zhao, C., Chen, S., Liu, Z., Huang, X., and Gao, Y.: WRF-Chem v3.9 simulations of the East Asian dust storm in May
1450 2017: modeling sensitivities to dust emission and dry deposition schemes, *Geosci. Model Dev.*, 13, 2125-2147,
1451 <https://doi.org/10.5194/gmd-13-2125-2020>, 2020.
- 1452 Zhang, Z. Y., Guan, H., Luo, L., Zheng, N. J., and Xiao, H. Y.: Response of fine aerosol nitrate chemistry to Clean Air Action in winter
1453 Beijing: Insights from the oxygen isotope signatures, *Sci. Total Environ.*, 746, 8, <https://doi.org/10.1016/j.scitotenv.2020.141210>, 2020.



- 1454 Zheng, B., Chevallier, F., Yin, Y., Ciais, P., Fortems-Cheiney, A., Deeter, M. N., Parker, R. J., Wang, Y. L., Worden, H. M., and Zhao, Y.
1455 H.: Global atmospheric carbon monoxide budget 2000-2017 inferred from multi-species atmospheric inversions, *Earth Syst. Sci. Data*,
1456 11, 1411-1436, <https://doi.org/10.5194/essd-11-1411-2019>, 2019.
- 1457 Zheng, B., Tong, D., Li, M., Liu, F., Hong, C. P., Geng, G. N., Li, H. Y., Li, X., Peng, L. Q., Qi, J., Yan, L., Zhang, Y. X., Zhao, H. Y.,
1458 Zheng, Y. X., He, K. B., and Zhang, Q.: Trends in China's anthropogenic emissions since 2010 as the consequence of clean air actions,
1459 *Atmos. Chem. Phys.*, 18, 14095-14111, <https://doi.org/10.5194/acp-18-14095-2018>, 2018.
- 1460 Zheng, Y. X., Xue, T., Zhang, Q., Geng, G. N., Tong, D., Li, X., and He, K. B.: Air quality improvements and health benefits from China's
1461 clean air action since 2013, *Environ. Res. Lett.*, 12, 9, <https://doi.org/10.1088/1748-9326/aa8a32>, 2017.
- 1462 Zhong, Q., Tao, S., Ma, J., Liu, J., Shen, H., Shen, G., Guan, D., Yun, X., Meng, W., Yu, X., Cheng, H., Zhu, D., Wan, Y., and Hu, J.: PM2.5
1463 reductions in Chinese cities from 2013 to 2019 remain significant despite the inflating effects of meteorological conditions, *One Earth*,
1464 4, 448-458, <https://doi.org/10.1016/j.oneear.2021.02.003>, 2021.
- 1465 Zhou, M., Nie, W., Qiao, L., Huang, D. D., Zhu, S., Lou, S., Wang, H., Wang, Q., Tao, S., Sun, P., Liu, Y., Xu, Z., An, J., Yan, R., Su, H.,
1466 Huang, C., Ding, A., and Chen, C.: Elevated Formation of Particulate Nitrate From N2O5 Hydrolysis in the Yangtze River Delta
1467 Region From 2011 to 2019, *Geophys. Res. Lett.*, 49, e2021GL097393, <https://doi.org/10.1029/2021GL097393>, 2022a.
- 1468 Zhou, W., Lei, L., Du, A. D., Zhang, Z. Q., Li, Y., Yang, Y., Tang, G. Q., Chen, C., Xu, W. Q., Sun, J. X., Li, Z. J., Fu, P. Q., Wang, Z. F.,
1469 and Sun, Y. L.: Unexpected Increases of Severe Haze Pollution During the Post COVID-19 Period: Effects of Emissions, Meteorology,
1470 and Secondary Production, *J. Geophys. Res.-Atmos.*, 127, 14, <https://doi.org/10.1029/2021jd035710>, 2022b.
- 1471 Zhou, W., Gao, M., He, Y., Wang, Q. Q., Xie, C. H., Xu, W. Q., Zhao, J., Du, W., Qiu, Y. M., Lei, L., Fu, P. Q., Wang, Z. F., Worsnop, D.
1472 R., Zhang, Q., and Sun, Y. L.: Response of aerosol chemistry to clean air action in Beijing, China: Insights from two-year ACSM
1473 measurements and model simulations, *Environ. Pollut.*, 255, 11, <https://doi.org/10.1016/j.envpol.2019.113345>, 2019.
- 1474